

Characteristics of turbulent flow around bridge abutments in the presence of vegetation in channel bed under ice-covered flow conditions

Sanaz Sediqi, Jueyi Sui^{*}, Guowei Li, Mauricio Dziedzic

School of Engineering, University of Northern British Columbia, Prince George, BC V2N 4Z9, Canada

ARTICLE INFO

Keywords:

Vertical-wall bridge abutment
Ice cover roughness
Flow field
Vegetation configuration pattern
Vegetation density
Sheath layer

ABSTRACT

During winter, ice cover frequently forms on the water surface of rivers with vegetated channel beds in cold regions. The investigation of the impacts of both ice cover and channel bed vegetation on flow structures around bridge abutments is essential for engineers to gain a comprehensive understanding of the complex interactions occurring in such a situation. In the present study, the flow structure around a rectangular bridge abutment in the presence of vegetation under ice-covered conditions has been studied. Considering different vegetation densities by arranging vegetation elements in square and staggered configurations, this study incorporates the influence of ice covers with different roughness, namely smooth and rough ice cover. Key turbulence parameters, including turbulence intensity, Reynolds shear stress (RSS), and turbulent kinetic energy (TKE), are also examined based on laboratory experiments. Results show that the shape of velocity profiles for flow over a vegetated channel bed changes from an S-shaped curve under an open flow condition to a convex shape under ice-covered conditions. The effects of an ice cover and vegetation on the flow around the bridge abutment create unpredictable turbulence intensity patterns. Under a rough-covered flow condition, there appears a larger area with negative Reynolds shear stress (RSS) downstream of the abutment. Turbulent kinetic energy (TKE) under ice-covered conditions has substantially lower magnitudes than in open flow conditions.

1. Introduction

Bridges are essential for safe and efficient transportation, and the abutments located at either end of a bridge assist in transferring the weight of the span to its foundation. A variety of research has been carried out to study the flow characteristics around bridge abutments by analyzing parameters such as flow velocity and shear stress (Molinias et al., 1998; Sui et al., 2010a). Melville (1997) studied the flow pattern around a bridge abutment and found that the flow in erodible beds is a complex three-dimensional turbulent flow. Ahmed and Rajaratnam (2000) observed considerable shear stress close to the abutment corners, up to 3.6 times larger than in the approaching flow. Barbhuiya and Dey (2003) measured the flow fields at different sections around vertical-wall abutments and reported the presence of a primary vortex associated with a down-flow upstream of the abutment and a reverse flow behind the abutment.

Engineers must consider the complexities of designing bridges when there is aquatic vegetation surrounding bridge abutments since the presence of vegetation dramatically affects flow fields in vegetated

rivers. Knowing the intricate flow structure around bridge abutments with submerged vegetation in the channel bed is essential to ensure structural soundness and optimal hydraulic performance.

To thoroughly understand the complex dynamics of the bridge abutment and surrounding vegetation, a number of experimental investigations, simulations, and field research have been conducted. Recently, researchers have been focusing on how submerged vegetation affects different environmental and hydraulic processes because of their impact on river ecosystems (Barahimi and Sui, 2023; Giacomazzo et al., 2023; Huai et al., 2019; Velle et al., 2022; C. Wu et al., 2023). Submerged vegetation patches provide habitat for aquatic organisms, prevent channel bed erosion, and improve water quality (Liu et al., 2022; Mo et al., 2017; Rameshkumar et al., 2019). Nokhbe Zaeim and Saneie (2022) conducted a laboratory investigation to assess the flow and scour process around bridge piers in the presence of abutment and vegetation. They analyzed the floodplain's vegetation density, measured by the percentage of vegetation cover, and concluded that it significantly influences the scour process. Kabiri et al. (2017) studied the flow structure over a wavy bed with vegetation cover. They pointed out that vegetation

^{*} Corresponding author.

E-mail addresses: sediqi@unbc.ca (S. Sediqi), jueyi.sui@unbc.ca (J. Sui), gli@unbc.ca (G. Li), mauricio.dziedzic@unbc.ca (M. Dziedzic).

<https://doi.org/10.1016/j.coldregions.2024.104172>

Received 31 July 2023; Received in revised form 14 February 2024; Accepted 5 March 2024

Available online 11 March 2024

0165-232X/© 2024 The Authors. Published by Elsevier B.V. This is an open access article under the CC BY license (<http://creativecommons.org/licenses/by/4.0/>).

cover considerably influences the flow structure and results in apparent flow separation and reattachment point. The law of the wall was not valid within the vegetation cover, but it fitted well to the zone above the vegetation cover within the inner layer. Afzalimehr et al. (2014) conducted an experimental study under two different channel conditions to assess the impacts of channel bank vegetation on velocity and Reynolds stress distributions around a wing-wall abutment. They found that the vegetated banks can cause a decrease in Reynolds stress (RS) near the bed and remove negative values of RS by undermining the unfavorable pressure gradient upstream of the abutment. Nabaei et al. (2021) investigated the effect of submerged vegetation on flow structure around a semi-circular abutment. They claimed that vegetation in the channel bed significantly reduces the primary vortex but has less impact on the wake vortex. In addition, they claimed that the tangential velocity, radial velocity, and Reynolds shear stress are reduced by the presence of vegetation in the channel bed.

To date, understanding of river hydrodynamics is mainly limited to the period of flow under open channel flow conditions. During winter, however, ice cover is a common occurrence in numerous rivers in cold regions, affecting flow conditions, as about half of the Earth's largest rivers experience seasonal ice cover (Theilman et al., 2021). The presence of an ice cover on the water surface can change the primary setting in which a hydraulic structure is built in a river, induce bed material removal around the structure, block waterway openings, and damage the structure by weakening the components and deteriorating the material.

Ice cover on the water surface has direct and indirect effects on directly and indirectly affects aquatic vegetation in flowing water. In winter, plants respond differently to the development of an ice cover depending on their traits. The ice cover on the water surface will be less damaging to plants whose budding parts are underground or sturdy with underground or sturdy budding parts, such as those with extensive root systems (Lind et al., 2014). Although the presence of an ice cover affects the submerged vegetation physiologically and lowers productivity, vegetation will not cease. Boylen and Sheldon (1976) determined the density of 26 different rooted submerged vegetation species under winter ice cover. It is found that nearly 40% of the vegetation taxa continued growing and even maintained their density. Results indicated that some vegetation species have different strategies to withstand the freezing period (Renman, 1989), and some vegetation species even survive as wintergreen and keep their foliage during the winter months (Nagao et al., 2005).

Results have shown that the presence of an ice cover on the water surface reduces the bulk velocity of the flow, increases flow depth, and significantly diminishes bed load transport (Ettema, 2002; Ettema et al., 1997; Sui et al., 2000, 2010b; Vandermause et al., 2021). Lindenschmidt et al. (2019, 2022) pointed out that river structures, particularly bridge components, when surrounded by ice cover, create an intricate interplay with the overall river flow. They found that during 1997–2002, many rivers in Germany, including the Oder River, faced severe floodings caused by ice jams. Following the floods, high sediment depositions occurred due to the significant transport of fine sediments. This initiated a cyclical process where vegetation growth accelerated because the plants filtered out the fine sediments (Dittricht and Järvelä, 2005). These occurrences highlighted the significance of studying the flow-vegetation-ice dynamics.

Due to the high risk of data acquisition in rivers under ice-covered conditions, researchers generally use laboratory flumes and physical models to study the hydraulic behavior of ice-covered flows, such as the flow characteristics, sediment transport, and morphological changes in ice-affected river systems. Zabilansky (2002) conducted some tests in a refrigerated flume to examine the flow under ice-covered conditions. Two types of ice covers (smooth and rough covers) were used in the study, with ice covers floating on the water surface. It was found that bed shear stresses increased under rough ice cover. Sui et al. (2009, 2010b) studied the effect of ice cover on flow characteristics. Their

results acknowledged that, under ice-covered flow conditions, the maximum velocity is located between ice cover and channel bed depending on the ratio of cover roughness to the bed roughness; the larger this ratio, the closer the maximum velocity shifted toward the bed. Jafari and Sui (2021) investigated the velocity fields and turbulent structures around spur dikes in the presence of ice covers with different roughness coefficients. Their results showed that an increase in ice cover roughness can increase 3D velocity component values and turbulence intensities.

In general, engineering design projects in rivers that experience ice problems are based on some simple assumptions, leading to the simplification of ice-covered fluvial hydraulics in river engineering studies. Considering that the presence of river ice should affect river morphology and ecology throughout the year, a better understanding of the fluvial hydraulics under ice-covered flow conditions is required.

To date, however, research work has never been reported regarding the simultaneous impacts of ice cover and vegetation on flow dynamics around hydraulic structures such as bridge abutments. Flow in an ice-covered channel over a vegetated bed can behave differently compared to that under the bare bed (or without vegetation in the channel bed) conditions. The characteristics of an ice-covered flow over a vegetated channel bed should be affected by various factors such as flow Froude number, ice cover roughness, vegetation configuration, vegetation density, and grain size of bed material. All these factors make it challenging to establish a general set of principles describing the role of the roughness of an ice cover on the water surface and the properties of vegetation patches in the channel bed.

By considering the simultaneous effects of an ice cover and submerged vegetation patch around a rectangular abutment, this research seeks to examine the impact of vegetation configuration and density on flow structure (including velocity distribution, turbulence intensity, Reynolds shear stress, and turbulent kinetic energy) around bridge abutments under ice-covered conditions. The leafless vegetation patch, which consists of many vegetation elements, represents a typical group of aquatic vegetation patch under ice-covered conditions in winter. By considering both ice cover and submerged vegetation as integral components of the flow dynamics, the present study seeks to shed light on their combined impact, providing a comprehensive understanding of the complex interactions between these elements and their effects on flow characteristics. The innovative findings of this study will bridge a critical research gap, resulting in more accurate modeling and improved management strategies for river engineering and infrastructure planning affected by ice cover on the water surface and vegetation on the channel bed.

2. Materials and methods

2.1. Flume and facilities

The experiments have been conducted in a flume at Quesnel River Research Center (QRRC), University of Northern British Columbia. The flume used is a large-scale outdoor flume that is 38.0-m long, 2.0-m wide, and 1.0-m deep with a streamwise slope of 0.2%, as shown in Fig. 1. There are two sandboxes in the flume that are considered the main experimental zones. Additional details about this flume used in this experimental study can be found in Li et al. (2023), as they utilized the same flume. Since vegetation patches in natural rivers grow in shallower parts of the rivers, an approaching flow depth of 24 cm (at the tailgate) was used in this study. The maximum flow rate for this experimental study was 130 L/s.

In the sandboxes, non-uniform natural sand with a median grain size (d_{50}) of 0.9 mm was filled as bed material. A rectangular model bridge abutment was made from plexiglass that can provide a clear view from inside the abutment. The model abutment, which was 0.2-m long (extended from the flume sidewall) and 0.4-m thick (along the flume sidewall), was installed in the middle of each sandbox. On the surface of

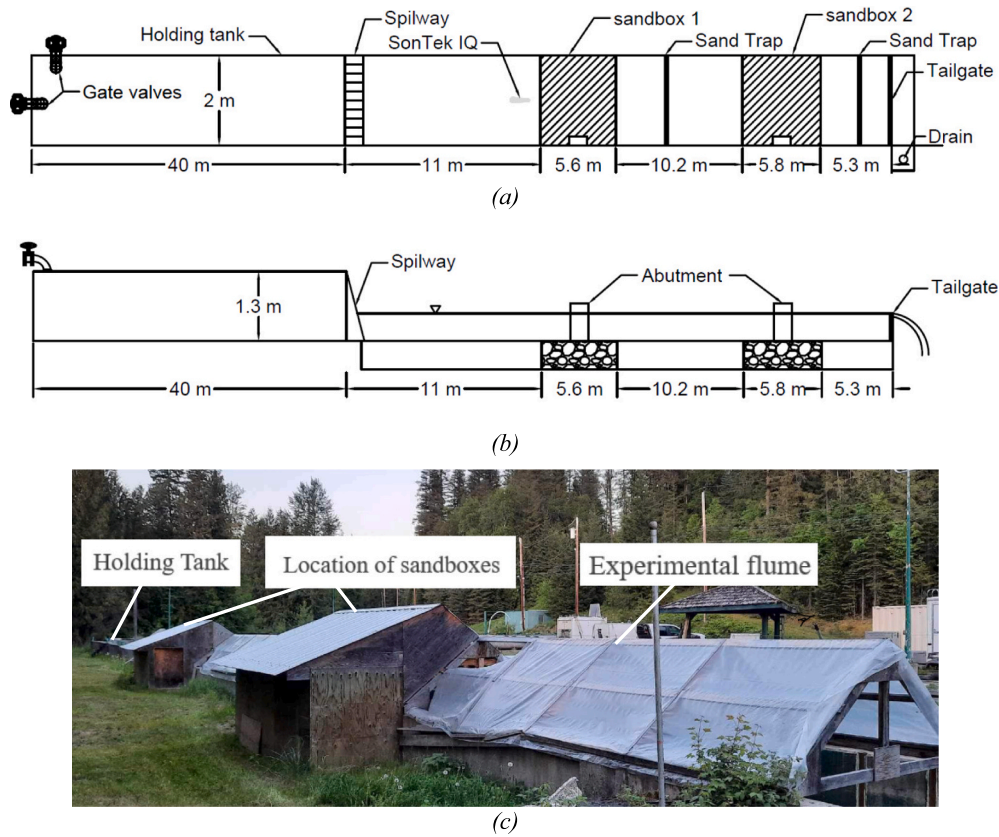


Fig. 1. (a) Plan view, (b) side view, and (c) a photo of the experimental flume, taken by Li et al. (2023).

the model abutment, measuring scale lines were marked for observations. A part of the abutment was buried in the sediment in the sandbox and kept as un-submerged for all experimental runs.

Vegetation patches within flow can be categorized into three classes: deeply submerged with the ratio of flow depth (H) to the height of vegetation (h) $H/h > 10$, shallow submerged ($H/h < 5$), and emergent ($H/h = 1$). In natural rivers, the majority of submerged aquatic vegetation falls within the range of shallow submergence. In this study, a leafless submerged vegetation patch was used. The vegetation patch, which consisted of numerous vegetation elements, was planted in the sand bed around the abutment. Vegetation elements were arranged in either a square pattern (Fig. 2a) or a staggered pattern (Fig. 2b). These configurations consist of two options for different spacing distances of 15 cm for higher and 20 cm for lower vegetation density. In total, these combinations yield four distinct placement patterns of vegetation elements. The population and canopy morphology of the vegetation patches are usually calculated using various methods and are very important due to the dependency of flow characteristics on these factors. The most common parameter to characterize rigid vegetation elements used in this study is the roughness density (λ) which is a non-dimensional measurement of canopy density and is the frontal area of plants per bed area. According to Nepf (2012), the roughness density (λ) is calculated using Eq. (1):

$$\lambda = ah \quad (1)$$

where h is the vegetation height, equal to 1.5×10^{-1} m for the experiments in this study, and a is the frontal area of plants per unit volume, known as vegetation density, which is considered as another common density parameter and defined as the following:

$$a = \frac{m\bar{A}_i}{h} \quad (2)$$

where m is the number of vegetation elements per unit area of the channel bed as presented in Table 1. \bar{A}_i is the mean frontal area of vegetation elements. From Eqs. (1) and (2), it can be concluded that the roughness density (λ) can be obtained from the product of the number of vegetation elements per unit bed area and the average frontal area of the plants ($\lambda = m\bar{A}_i$). Considering $\bar{A}_i = 3.3 \times 10^{-3} \text{m}^2$ as the average frontal area of the vegetation elements used in this study, the calculated a and λ values are listed in Table 1. \bar{A}_i was computed using MATLAB image processing software derived for a single vegetation element.

The relatively small dispersion of vegetation elements for this study is selected based on the situation of submerged vegetation in streams under the ice-covered flow conditions because the abundance of vegetative units is affected during winter to some extent, causing the dispersed distribution (Renman, 1989; Virtanen et al., 2001).

Each model vegetation element consists of one stem and several branch clusters (each cluster has three branches). Given that this experimental study aims to simulate fluvial hydraulics in the presence of ice cover, the model vegetation patch comprised leafless vegetation elements, as shown in Fig. 3. The vegetation height (h) was 15 cm to create the submergence ratio (H/h) of 1.3 in all experimental runs and resemble the real situations in nature since the aquatic canopies in rivers have a limited submergence ratio of $1 < H/h < 2$ (Nepf and Vivoni, 2000). The submergence depth is important to indicate the dominant factor for momentum transfer. Inside the vegetation canopy, the pressure gradient causes stress-driven flow, and the bed slope results in potential-driven flow. The contribution share of these factors in momentum transfer is proportional to the $(H-h)/h$ ratio. For $H/h = 1.3$, the flow is mainly driven by the bed slope (Potential-driven flow) with a small contribution of the pressure gradient and stress (Nepf et al., 2007).

When the primary focus is not on structural integrity, robust and rigid materials such as plywood and Styrofoam panels have been proven to be effective for simulating ice cover conditions, as indicated by

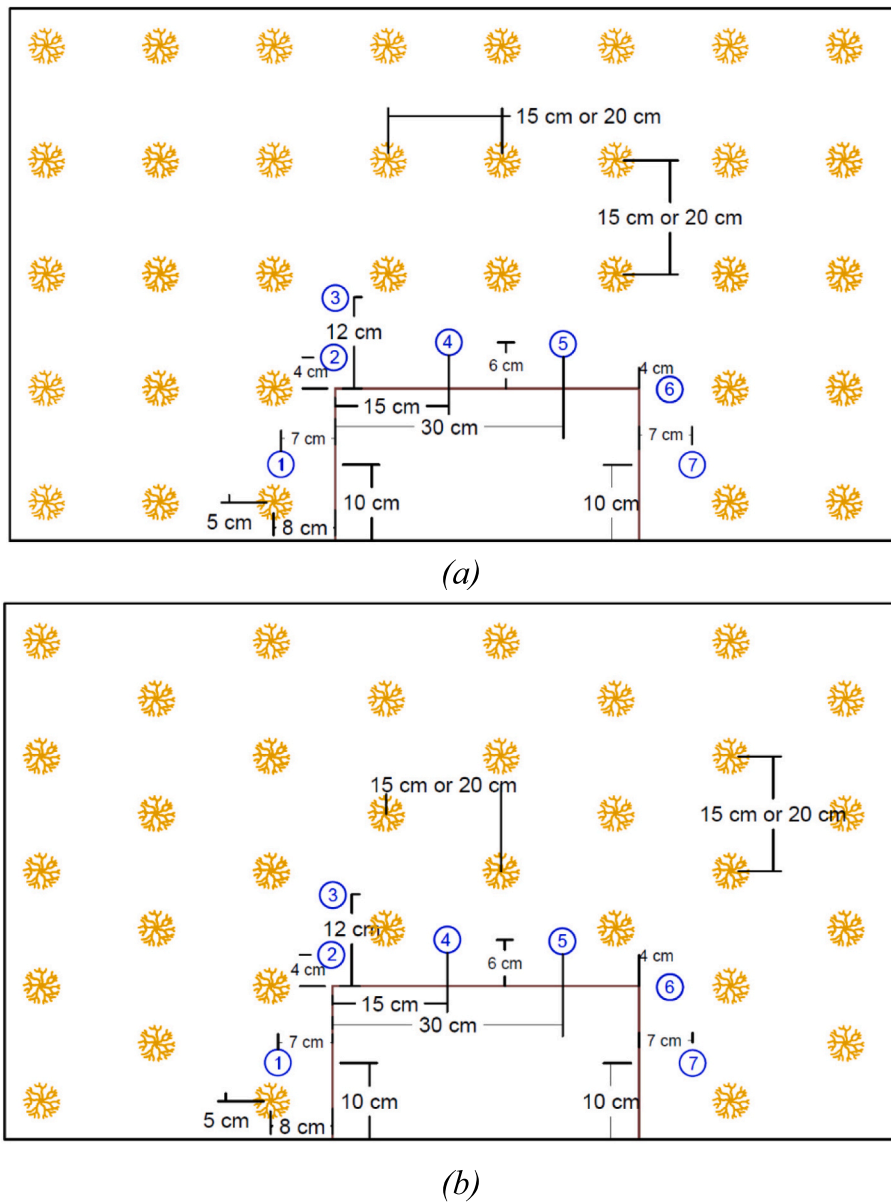


Fig. 2. Layout of the vegetation configurations in the sandbox and the ADV positions around the abutment and the vegetation elements in (a) square configuration and, (b) staggered configuration. Location 1, upstream of the abutment where the downflow happens; locations 2, 3, and 6, close to the abutment corners where high turbulent flow is expected, locations 4 and 5, along the tip of the abutment, and location 7, downstream of the abutment - the wake zone.

Table 1
Vegetation parameters for different setups.

Vegetation arrangement	m (m^{-2})	a (m^{-1})	λ
Square configuration	49	1.078	0.161
	36	0.792	0.118
Staggered configuration	49	1.078	0.161
	33	0.726	0.108

previous research (Hanis and Zabilansky, 2004; Peters et al., 2017; Wu, 2015; Wu et al., 2014, 2015, 2016). In this context, the primary consideration for the ice cover simulation is surface roughness, and this study incorporated Manning's coefficient to address this aspect. Styrofoam panels were used to model ice cover. Each panel is 1.95-m long, 1.20-m wide, and 0.025-m thick. Two types of ice cover were used, namely, smooth and rough ice cover. The smooth cover was simulated using smooth Styrofoam panels without any treatment, while the rough cover was modeled by attaching small cubes of Styrofoam to the

underside of the panels (Fig. 3). Each Styrofoam cube has dimensions of $25 \text{ mm} \times 25 \text{ mm} \times 25 \text{ mm}$. Numerous Styrofoam cubes were attached to the bottom of the panels with the staggered arrangement, and the spacing distance between the 2 adjacent cubes is 35 mm (all dimensions with $\pm 5 \text{ mm}$ error). During each experimental run, the model ice cover on the water surface floats freely with the change of flow depth.

To obtain a representative description of flow velocities around the abutment in the presence of both vegetation and ice cover, the instantaneous 3D velocity components were measured at different locations around the abutment using a down-looking SonTek 10-MHz Acoustic Doppler Velocimeter (ADV) with the accuracy of 1%, $\pm 0.25 \text{ cm/s}$. The ADV sampling volume was 250 mm^3 . The sampling volume takes on a cylindrical shape, aligned with the axis of the acoustic transmitter. This cylinder measures approximately 6 mm in diameter and 9 mm in length. Due to the limitation of the ADV, measurements of flow velocities have been carried out from the channel bed to a depth 10 cm below the water surface, with a vertical distance of 10 mm between adjacent measurement points. The duration for collecting data at each point was 120 s.

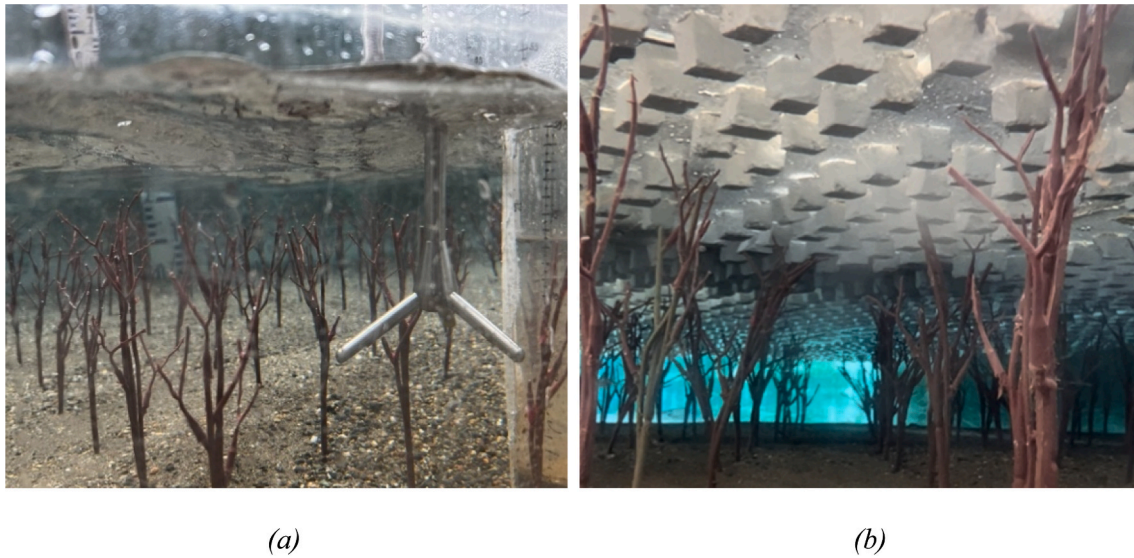


Fig. 3. Measuring flow properties using ADV in the presence of vegetation around the abutment in (a) open channel flow and (b) rough ice-covered flow.

Aberrant data with an SNR of <15 dB and a correlation coefficient of <70% were filtered out by means of the WinADV software (Caroppi et al., 2020).

In total, seven locations (Fig. 2) for the ADV measurements around the abutment were selected to acquire data to assess the velocity fields and turbulent characteristics. The vegetation elements around the abutment do not interfere with the sampling volume and the path of the acoustic beam of the ADV. To allow comparisons, the ADV measurement locations for all experiments were at the same relative position to the abutment. A well-defined coordinate system was established to guarantee the precise placement of the ADV for data acquisition. The origin of this coordinate system was set at the zero-height level or the initial bed level ($z = 0$), positioned 70 cm upstream of the front side of the abutment ($x = 0$), and aligned with the channel wall ($y = 0$). The instantaneous velocity components in three directions acquired using the ADV can be used to calculate mean velocity, shear stresses, turbulence intensity, Reynolds shear stress, and turbulent kinetic energy for describing the flow.

In addition, a SonTek IQ, which is a monostatic Doppler current meter, was used in this study. This device was mounted 2 m upstream from the first sandbox, recording >100 samples for each experimental run. The data collected using SonTek IQ was used to determine mean flow velocity, water depth, and flow discharge accurately.

Dynamic similarity necessitates that, beyond geometric and kinematic similarities, all force ratios in the system are identical (Heller, 2011). Given the inherent complexity of replicating all force ratios accurately, scale effects become an inevitable consideration. However, as in this study, Froude number similarity is employed to mitigate these effects effectively. The criterion $Fr_{model} = Fr_{prototype}$ is a frequent application in the context of open-channel hydraulics, with Froude number similarity particularly suited for modeling turbulent phenomena. The non-dimensional maximum scour depth values (d_s/h) connection with the Froude number was closely tracked, revealing that the d_s/h -value fits well across a range of Fr , despite variations in other factors.

Flow regimes in the presence of a vegetation patch or a group of vegetation elements can be assessed using the vegetation Reynolds number. A vegetation patch's characteristic length scale or the average diameter of each vegetation element is considered when assessing flow conditions (Tanino and Nepf, 2008). Vegetation Reynolds number (Re_d) was calculated using Eq. (3).

$$Re_d = \frac{Ud}{\nu} \quad (3)$$

where U is the streamwise averaged flow velocity, ν is the kinematic viscosity, and d is the stem vegetation diameter (D'Ippolito et al., 2022; Van Veelen et al., 2020). To obtain the average stem diameter of the vegetation elements, the number of stems and branches was counted, their widths were measured, and the average value was computed. Results of calculations of Reynolds number and flow Froude number indicated that all flows in the vegetated section for different experimental runs in this study belong to fully developed turbulent and sub-critical flows.

2.2. Experimental procedure

The same procedure was strictly followed for all experimental runs to ensure the repeatability of the experiments. Since this flume is a large-scale outdoor flume, some parameters, such as water viscosity and temperature, were not controllable.

Equilibrium scour depth is reached when the dimensions of a scour hole stabilize over time. Different criteria help identify this state. Melville and Chiew (1999) proposed that the approximate equilibrium is achieved when scour depth variation is <5% of the width of bridge abutments. Oliveto and Hager (2002, 2005) revealed that the pivotal factor governing the scour process is the densimetric particle Froude number and found that the temporal evolution of local scour development is predominantly influenced by the geometrical variables of hydraulic parameters, in-stream structures, and granulometric characteristics. Subsequently, Kothiyari et al. (2007) refined Oliveto and Hager's findings and developed a more precise relationship for the temporal evolution of the maximum scour depth around the bridge pier and abutment. Applying their relationship, the estimated time required to reach an equilibrium scour condition for this study is projected to be <6 h.

However, it's worth noting that local scour under ice-covered flow conditions introduces a level of complexity compared to that in open-channel flow scenarios. Extensive experiments have been conducted to study local scour around bridge abutments (Wu et al., 2014, 2015, 2016) and side-by-side piers (Namaee and Sui, 2020) under ice-covered flow conditions using the same flume, bed sediments, and model ice cover as in this study. They stated that a quasi-equilibrium scour can happen within the first 6 h of the experiment, and there was no change in the scour hole pattern after 12 h. To ensure an equilibrium scour condition could be achieved, the experimental runs for this study lasted 24 h.

In the present study, the following procedures for data acquisition

were followed for all experimental runs:

- 1) After installing the abutment and arranging vegetation elements in the sandbox, the sandboxes were carefully leveled. Then, the upstream water holding tank was filled. Afterward, all Styrofoam panels (or model ice cover) were carefully placed side by side on the flume bed.
- 2) Then, by gradually opening the valves, the water from the upstream holding tank was slowly fed into the flume to prevent initial erosion at the abutment. The flow depth in the flume raised gradually, and the model ice cover floated on the water surface. Once the approaching water depth reached the required value, the valves were opened to provide the required flow rate. During each experimental run, the water level, flow rate, and approaching velocity were monitored and calculated using the SonTek-IQ. In the meantime, the flow depth was recorded using a staff gauge in the middle of the sandboxes.

After a period of 24 h for each experiment, the experiment is considered to reach the equilibrium condition. Then, the ADV was carefully put inside the flow to measure the velocity field at various locations around the abutment. After all required measurements for flow velocity were completed, all valves were shut down. Then, the model ice cover was carefully removed from the water surface. Water in the flume was drained slowly by carefully adjusting the tailgate to avoid disturbing the deformation patterns of the channel bed.

In this study, experiments were conducted under the open channel, smooth ice-covered, and rough ice-covered flow conditions in the presence or absence of vegetation with different arrangement patterns and densities. Finally, the collected data were processed to assess the effect of the roughness of the ice cover as well as vegetation configuration and density on the flow characteristics around the bridge abutment. Table 2 outlines the conditions under which the experimental runs were conducted.

3. Results and discussion

3.1. Velocity distributions

Although the flume and the sandboxes are long enough to allow the flow to achieve a fully developed flow, the change in bed roughness from the sand bed to the vegetated patch resulted in the development of a new

Table 2
Summary of experimental runs.

Run No.	Vegetation configuration and density	Flow condition
1	Bare bed	Open channel
2		Smooth ice cover
3		Rough ice cover
4	Lower vegetation density	Open channel
5		Smooth ice cover
6		Rough ice cover
7	Square configuration	Open channel
8		Smooth ice cover
9		Rough ice cover
10	Higher vegetation density	Open channel
11		Smooth ice cover
12		Rough ice cover
13	Staggered configuration	Open channel
14		Smooth ice cover
15		Rough ice cover

boundary layer. Results of velocity profiles along the centerline of the flume at three consecutive cross sections in the channel reach upstream of the experimental zone showed similar patterns, implying a fully developed flow condition was achieved.

As mentioned by many researchers, near the vegetated bed, there is always considerable noise in the velocity data which must be discarded herein (Huai et al., 2019; Kazem et al., 2021; Nezu and Sanjou, 2008; Shivpure et al., 2016). The depth of this region in experiments was within 1.5 cm. On the other hand, due to the limitations of the ADV used in the experiments, the velocity data 10 cm near the water surface could not be collected.

In the following figures, the flow depth of $z/H = 0$ represents the initial bed level before the scouring process started, the negative z/H values represent positions within the scour hole, and u represents the time-averaged streamwise velocity component.

Fig. 4 shows the dimensionless time-averaged streamwise velocity profiles under open channel flow conditions in the presence of vegetation and on a bare bed. The velocity magnitudes are normalized using the maximum velocity (u_{Max}). In the upstream region and along the abutment outer sidewall, in the presence of the vegetation elements placed in the bed in square configuration, the streamwise velocity near the bed (particularly within the zone of vegetation stems) is lower for the higher vegetation density ($\lambda = 0.161$) than those for both the sparse square arrangement ($\lambda = 0.118$) and the bare bed. In the cases of the staggered arrangement, the near-bed velocity mainly depends on the locations of the profiles around the abutment. For example, it was observed that the near-bed velocity has lower magnitudes for the case of sparse square arrangement compared to that of the bare bed upstream of the abutment, while it has slightly higher values at location 5.

Despite the variations in velocity magnitudes near the bed, the profiles in all scenarios, both vegetated and non-vegetated beds, exhibit a converging trend until they intersect at a flow depth where z/H is < 0.3 . Furthermore, the flow velocity profile in the presence of vegetation in the bed show a pronounced peak below this depth. It's important to note that the flow depth of $z/H = 0.3$ corresponds to the location where the vegetation nodes begin to split into branches.

Disregarding minor fluctuations, the velocity profiles for the case of flow in the bare bed channel exhibit an increasing trend from the bed until z/H reaches about 0.15, after which they stabilize and maintain a constant trend within the recorded depth. In the presence of vegetation in the bed, in the zone below $z/H = 0.3$ along the abutment side and downstream of the abutment, the velocity profiles follow an increasing trend until reaching their peak and then a decreasing trend. The rate at which velocity changes across the flow depth at a specific location around the abutment in vegetated scenarios is mainly influenced by the vegetation configuration. The velocity reduction is more pronounced in the staggered arrangement compared to the square configuration.

Results of experiments showed that the configuration pattern of vegetation has more impact on velocity than that of vegetation density. Vegetation elements arranged in a staggered configuration had a greater effect on the velocity reduction compared to that of the square configuration. The reduction in the streamwise velocity results from the increase in the resistance to flow due to the presence of vegetation in the channel bed. The vegetation in the bed acts as a barrier and leads to flow separation in the wake zone of individual vegetation elements. As depicted in Fig. 2b, location 5 is situated nearly in line with vegetation elements arranged in the staggered configuration. In contrast, for the case of vegetation arranged in the square configuration, location 5 is positioned within the "channel" between the rows of vegetation elements. Thus, the variation in vegetation arrangements influences the corresponding velocity profiles.

The presence of vegetation arranged in the staggered configuration resulted in a complex flow field, enhancing velocity reduction compared to the square arrangement pattern. In the staggered configuration, the flow is more obstructed than that for the squared arrangement because the flow has to navigate through a more irregular arrangement of

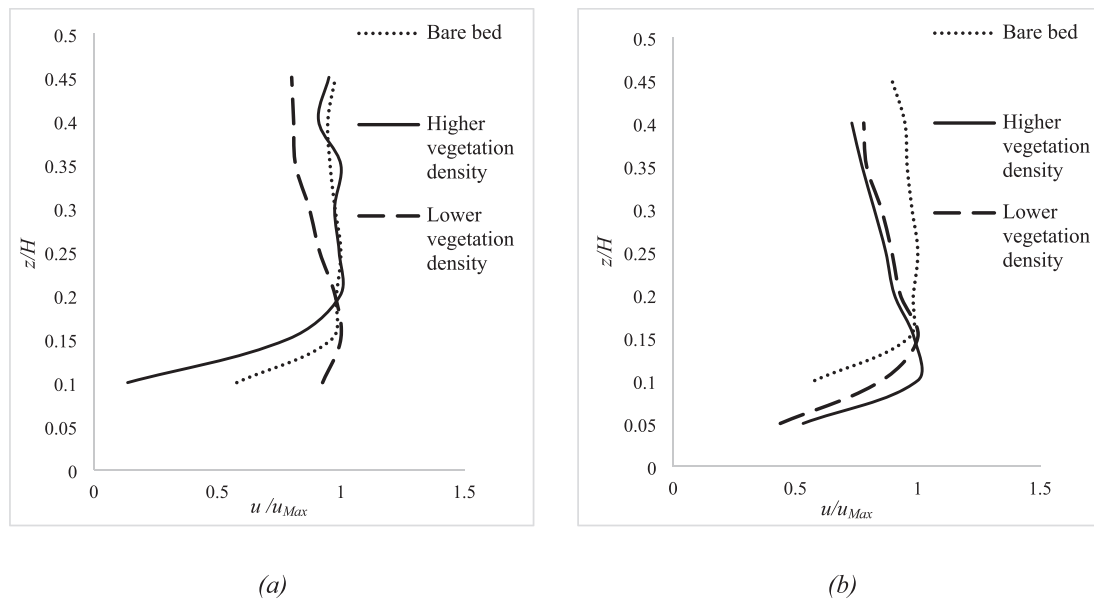


Fig. 4. The dimensionless time-averaged streamwise velocity profiles in non-vegetated open channel condition compared to those in open channel with vegetation patch with different vegetation densities at location 5 for (a) square arrangement of vegetation, and (b) staggered arrangement of vegetation.

vegetation elements, leading to an increase in drag and a decrease in velocity. In fact, the flow passes through the gaps between vegetation elements, with a longer delay associated with the staggered configuration.

The impact of the spatial distribution of vegetation elements on velocity reduction and flow patterns is also illustrated in Fig. 5. The time-averaged streamwise velocity contours at the horizontal plane (X-Y plane) around the abutment for the flow depths of $z/H = 0$ show that the velocity values close to the upstream edge of the abutment are within the range of $[-4-16]$, $[0-20]$, and $[0-12]$ for the bare bed, squared arrangement of vegetation, and staggered arrangement of vegetation, respectively.

At $z/H = 0$, in the presence of vegetation elements arranged in a square configuration, the velocity magnitude increased by about 25% compared to bare bed. However, for vegetation elements arranged in a staggered configuration, the velocity magnitude decreased by at least 25% compared to that without vegetation.

At the flow depth of $z/H = 0.4$, in the case without bed vegetation, the density of velocity contour lines in the downstream zone of the abutment is higher than that of the vegetated bed. In other words, velocity gradients are smaller in the downstream zone of the abutment for the vegetated bed cases, especially in the case of the staggered configuration, indicating the presence of vegetation increases the flow resistance.

It was observed that the velocity and the scour hole depth around the abutment were proportional and adversely related. The velocity decreased in locations where the depth of the scour hole is greater because of an increase in flow cross-sectional area. This finding is in good agreement with Nabaee et al. (2021). Fig. 6 shows a 3D view of the velocity contour around the abutment at flow depths of $z/H = 0$ and $z/H = 0.4$. At the upper left corner of the abutment, the streamwise velocity reaches its minimum magnitude, corresponding to the maximum depth of the scour hole. This phenomenon becomes increasingly more pronounced in close proximity to the bed. The velocity in deeper flow is affected by large vortices that are formed via Kelvin-Helmholtz (K-H) instabilities which are the dominant factor in transport in that layer, highlighting the complex interaction between flow dynamics and instability-driven phenomena. Although not directly recorded, the presence of the Kelvin-Helmholtz instabilities can be anticipated due to the alterations in flow velocity at varying depths caused by the influence

of vegetation and drag discontinuity (Nepf et al., 2007).

A secondary current is usually the main driver moving high-momentum water from the free surface to the channel bed and the low-momentum water from the bank to the central zone of the channel. The boundary shear stress increases when a secondary current moves away from the bank. On the contrary, when a secondary current moves toward the bank, the boundary shear stress decreases (Afzalimehr et al., 2011). The aspect ratio, defined as the ratio of the channel width to the flow depth of the channel, in the present study was 10.5, indicating a wide channel flow ($W/H > 5$). This means that the impact of secondary currents resulting from sidewall effects can be neglected and that the maximum flow velocity under an open flow condition occurs at the water surface because the vortices caused by side walls are damped quickly by moving away from them (Jing et al., 2019).

The velocity profiles in the presence of vegetation under an open flow condition are compared to those under an ice-covered flow condition in Fig. 7. In addition to the effects of the abutment and vegetated bed on flow velocity, the presence of an ice cover, which introduces a new flow boundary, influences the shape of velocity profiles. Under ice-covered flow conditions, similar to results under open flow conditions, the velocity profiles at different locations around the abutment differ. However, in all cases, at least one peak velocity exists in velocity profiles. Affected by the locations for measuring velocity around the abutment, the amount of the velocity peak varies. Under an open flow condition, one velocity peak occurs in the “sheath layer”, namely, in the zone below the nodes of vegetation elements ($z/H < 0.3$). The frontal width of vegetation elements is the least in this zone, and water passing through this layer experiences a larger net cross-sectional area for flow (Chen et al., 2011). Thus, the first peak of velocity profiles near the channel bed for all flow conditions is attributed to the effect of the sheath layer. The second peak of velocity profiles under an open flow condition should occur at the water surface ($z/H = 1$), since the flow in the present study belongs to a wide channel flow. According to reported studies, flow in the zone above the vegetation canopy under open flow conditions is expected to have a sharp increase in velocity toward the water surface.

Under the ice-covered flow condition, similar to the open flow condition, the first peak of velocity profiles occurs in the sheath zone. Under rough ice-covered conditions, the first peak of velocity profiles in the sheath zone upstream of the abutment displays a more pronounced

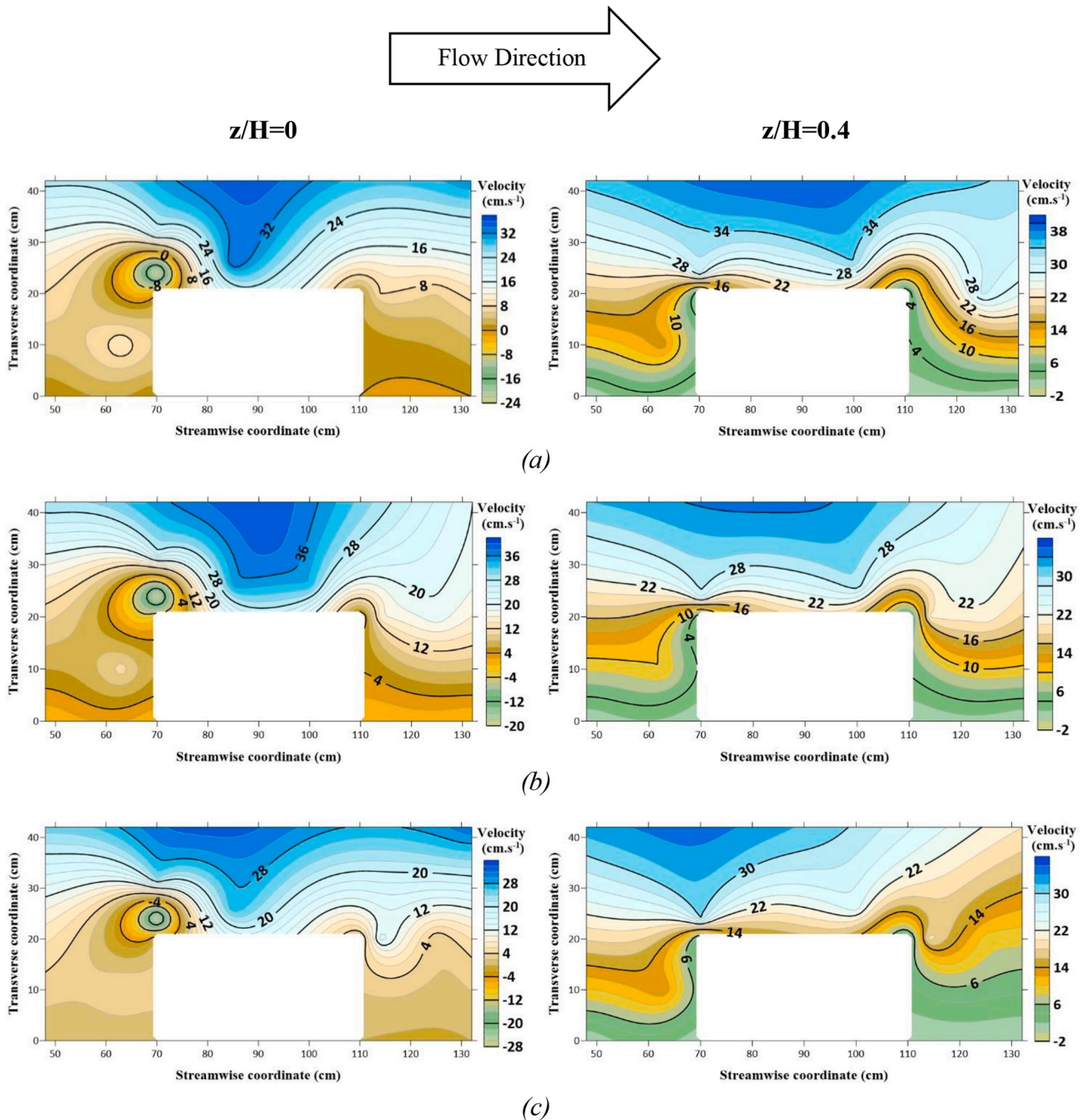


Fig. 5. Contour maps of streamwise velocity in open channel condition at (a) bare bed, (b) vegetated bed with square configuration and lower vegetation density, and (c) vegetated bed with staggered configuration and lower vegetation density at $z/H = 0$ (left panels) and $z/H = 0.4$ (right panels).

magnitude compared to those under both open channel and smooth-covered flow conditions. This difference is attributed to the larger relative roughness of the rough cover compared to a smooth-covered condition. The second peak of the velocity or the maximum velocity, under ice-covered conditions, is predicted to be located at a certain distance between ice cover and vegetation canopy, and an increase in the ice cover roughness leads to a further shift of the maximum velocity toward the vegetation canopy.

Under the condition of the same flow depth and discharge, since the maximum flow velocity under the rough-covered flow condition is larger than that under the smooth-covered flow condition, the velocity gradient under the rough-covered flow condition is larger than that for the case of smooth-covered flow.

Under an open flow condition and the presence of vegetation in the

channel bed, the velocity profile can be divided into three main zones: the emergent or canopy zone, within the stems of plants, the mixing layer zone, close to the top of the canopy, and the log-law zone, close to the water surface. It is reported that the streamwise velocity profile in the presence of a vegetation patch in a channel bed has an “S”-shaped curve (Huai et al., 2019; Kazem et al., 2021; Nezu and Sanjou, 2008).

In the presence of vegetation in the channel bed, the flow under an ice-covered flow condition can also be divided into three layers. The first layer, near the bed up to the nodes of vegetation elements – the sheath layer – experiences the first peak of velocity profiles. Moving to the second layer, which covers the flow depth from the nodes of vegetation elements to the top of the vegetation canopy, the influence of ice cover on velocity profiles becomes more pronounced. Flow velocity inside this layer decreases due to the increased resistance caused by the increased

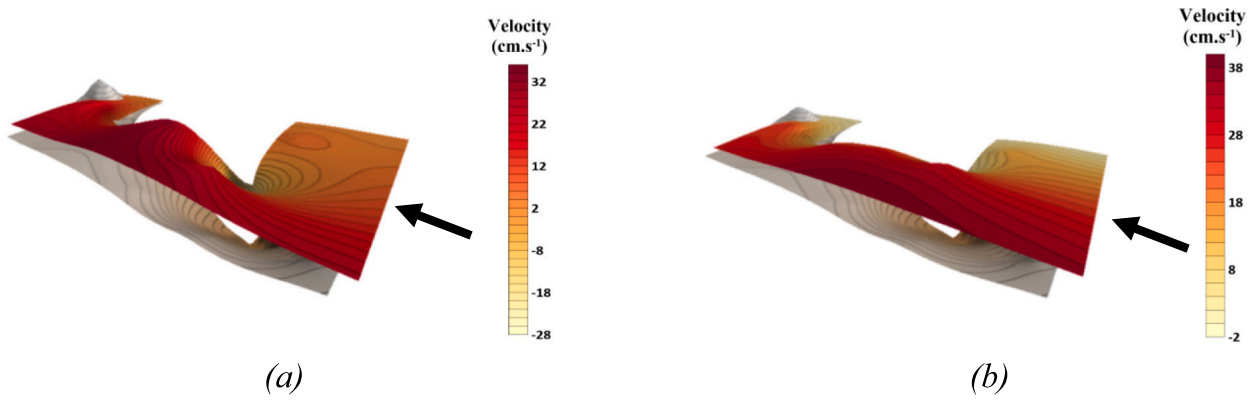


Fig. 6. 3D view of streamwise velocity contours over the 3D scour contour profile under an open channel condition in the presence of dense vegetation arranged in a staggered pattern: (a) $z/H = 0$ (left), and (b) $z/H = 0.4$ (right). (The arrows show flow direction).

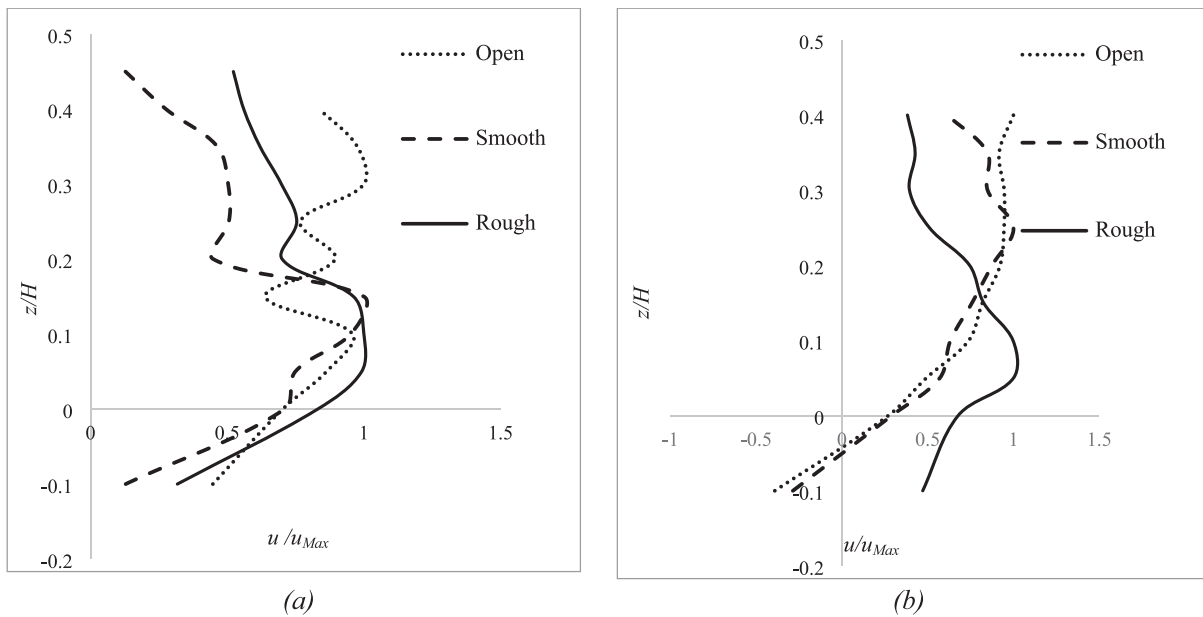


Fig. 7. The dimensionless streamwise velocity profiles under open channel, smooth ice-covered, and rough ice-covered flow conditions in the presence of vegetation in (a) square configuration, and (b) staggered configuration with higher vegetation density at location 1 (upstream of the abutment).

frontal area of vegetation elements. Also, since there are many vegetation branches presented irregularly in this layer, velocity profiles in this layer show variation. Under rough ice-covered flow conditions, a second peak in velocity profiles occasionally occurs around the top of the vegetation canopy with low vegetation density. This is due to the shift of the maximum velocity resulting from the high resistance of the rough ice cover. Finally, in the third layer, the flow velocity above the top of the vegetation canopy is anticipated to approach zero near the ice cover. Flow in this layer should be similar to the distribution pattern of the velocity profile under an ice cover without bed vegetation (Sui et al., 2010b). The velocity gradient in this layer should depend on the relative roughness of ice cover to that of the vegetation canopy, the location around the abutment, as well as vegetation configuration and density. As a result, the velocity profile in a vegetated bed under ice-covered conditions displays a convex shape. It should be noted that data collection using ADV in the third layer, from the top of the vegetation canopy to the water surface or ice cover, was not possible due to the limitations of the measurement instrument.

In the presence of vegetation, regardless of the arrangement patterns, Fig. 8 compares velocity profiles in vertical direction under the open channel, smooth ice-covered, and rough ice-covered flow conditions at

location 1 (upstream of the abutment). The presence of the abutment results in a powerful downward flow upstream of the abutment, referred to as “downflow”, which induces negative velocity in the vertical direction close to the abutment wall. The higher resistance of a rough ice cover reduces the streamwise flow velocity as it encounters the upstream side of the abutment and, consequently, the downflow intensity. This, in turn, leads to a corresponding decrease in the absolute magnitudes of the vertical velocity components near the abutment region. In other words, under an open channel flow condition, the presence of a stronger downflow due to non-covered flow leads to larger magnitudes of negative vertical velocities. Under an ice-covered flow condition, however, particularly the rough-covered flow condition, the larger resistance generated by an ice cover results in a reduction in the magnitudes of the vertical velocity components near the abutment wall.

3.2. Turbulence intensity. Turbulence intensity refers to fluctuations in velocity and can be expressed as a percentage of the mean velocity. The flow velocities in the stream-wise (u), lateral (v), and vertical (w) directions were decomposed into time-averaged (\bar{u} , \bar{v} , and \bar{w}) and turbulent components (u' , v' , and w'). The velocity fluctuations in three directions are obtained using the measured 3D instantaneous velocity, and the turbulent intensities are

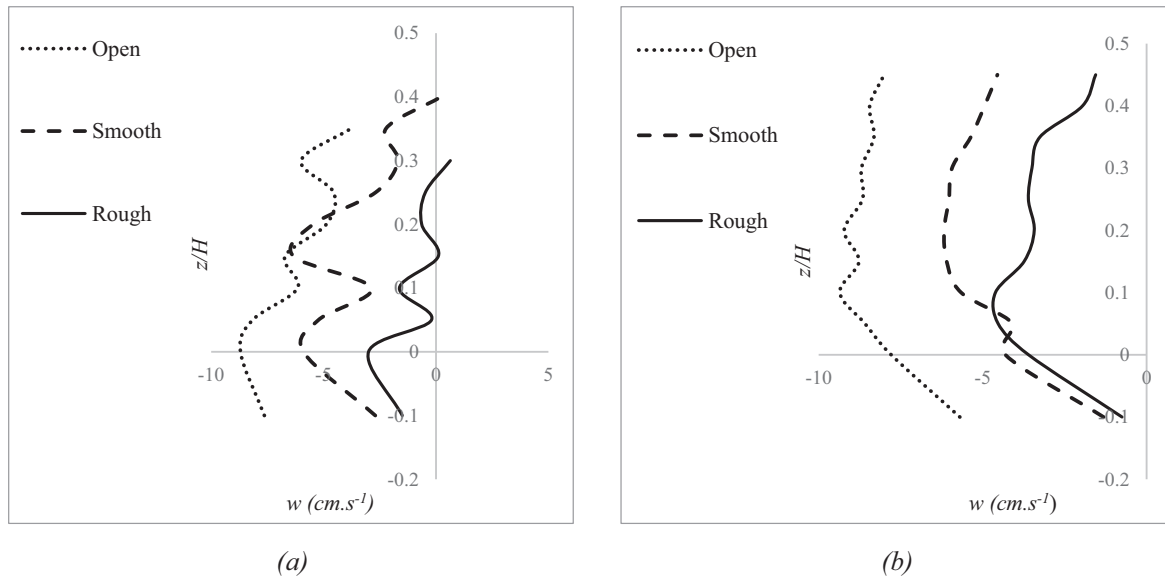


Fig. 8. The velocity profiles in vertical direction under open channel, smooth ice-covered, and rough ice-covered flow conditions in the presence of vegetation in (a) square configuration, and (b) staggered configuration with higher vegetation density at location 1 (upstream of the abutment).

calculated by RMS (Root-Mean-Square) (Eq. (4)).

$$\sqrt{u'^2} = u_{RMS}, \sqrt{v'^2} = v_{RMS}, \sqrt{w'^2} = w_{RMS} \quad (4)$$

u_{RMS} , v_{RMS} , and w_{RMS} are the Root Mean Square of fluctuations of velocity in streamwise, transverse, and vertical directions, respectively. The shear velocity (u_*), also known as friction velocity, is a primary parameter to measure the average velocity and, in this study, is used to normalize the turbulence intensity parameter. The shear velocity can be calculated in several ways. In the boundary layer method, shear velocity is computed using Eq. (5),

$$u_* = \frac{(\delta_* - \theta)u_{Max}}{C\delta_*} \quad (5)$$

where, u_{Max} is the maximum velocity, δ_* is the boundary layer displacement thickness, θ is the momentum thickness of the boundary layer that indicates the loss of momentum in the boundary layer, and C is an empirical coefficient adopted here as 4.4 for sandy beds (Afzalimehr and Rennie, 2009). Parameters δ_* and θ can be calculated using Eqs. (6) and (7), respectively,

$$\delta_* = \int_0^H \left(1 - \frac{u}{u_{Max}}\right) dy \quad (6)$$

$$\theta = \int_0^H \frac{u}{u_{Max}} \left(1 - \frac{u}{u_{Max}}\right) dy \quad (7)$$

The contour maps of non-dimensional streamwise turbulence intensities (u_{RMS}/u_*) for open channel cases and the vertical distributions of non-dimensional streamwise turbulence intensities upstream of the abutment for open channel flow compared to those of ice-covered flow conditions are illustrated in Figs. 9 and 10, respectively.

Near the abutment, the turbulence intensity is usually higher than in the undisturbed flow because the flow encounters resistance and undergoes shearing as it passes over the abutment wall. The turbulence intensity is highest near the corners and edges of the abutment. These locations experience more intense flow separation and higher vorticity, resulting in increased turbulence. The turbulence intensity reaches higher values in the wake regions downstream of the abutment, where flow separates and vortices form. The turbulence intensity gradually decreases as flow moves away from the corners. Interaction between the

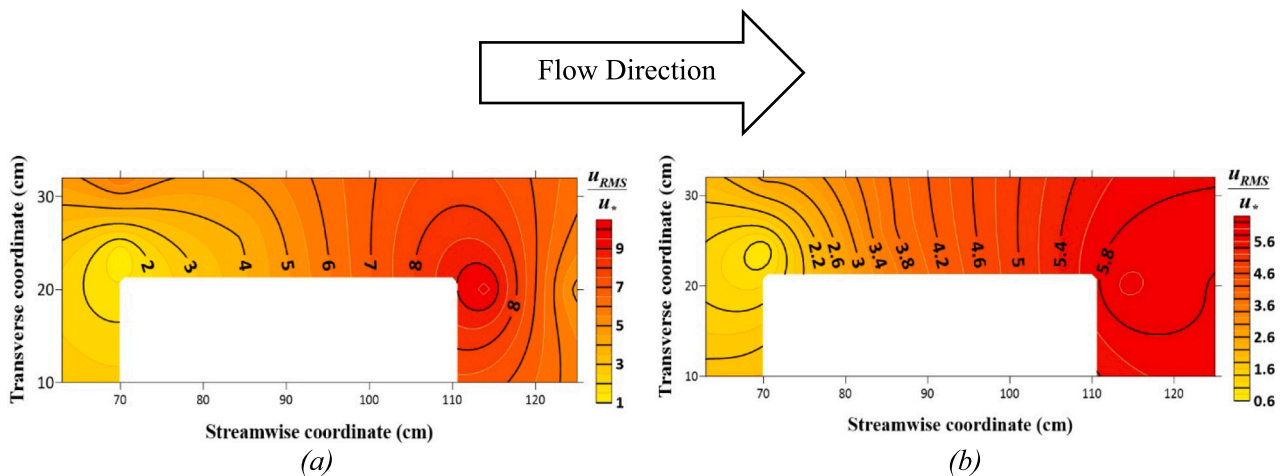


Fig. 9. Contour map of normalized streamwise turbulence intensities around the abutment in open channel condition at $z/H = 0$ for: (a) vegetation elements arranged in a square configuration with lower density and (b) vegetation elements arranged in a staggered configuration with lower density.

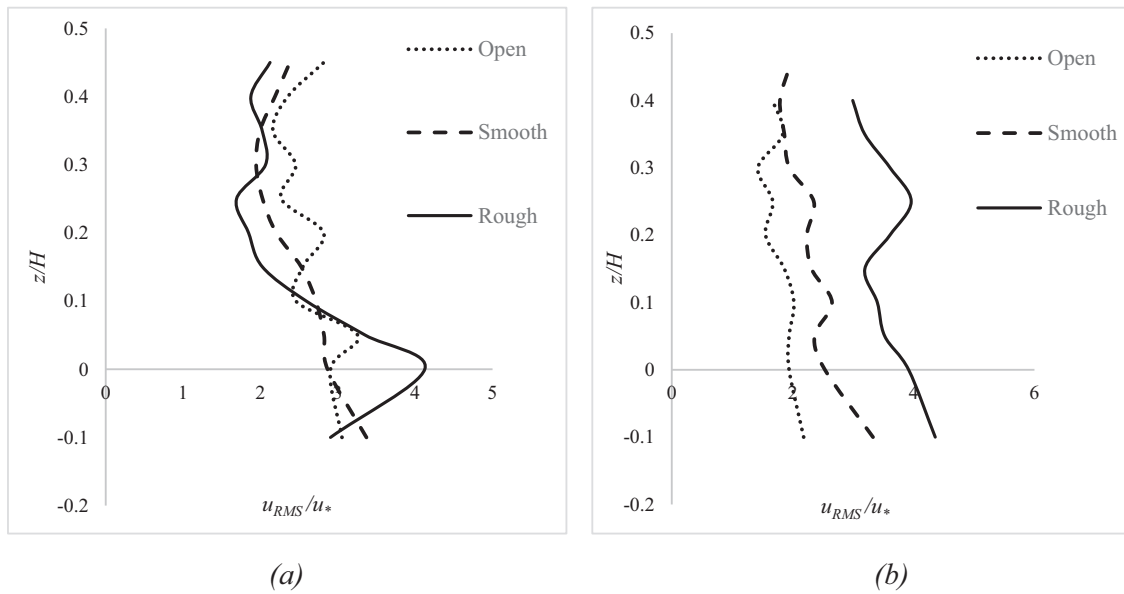


Fig. 10. Vertical distribution of non-dimensional streamwise turbulence intensities upstream of the abutment (location 1) under open channel, smooth ice-covered, and rough ice-covered flow conditions in the presence of vegetation in (a) vegetated bed arranged in square configuration with lower density and (b) vegetated bed arranged in a staggered configuration with lower density.

main flow and the reversal flow created in the slant bed near the abutment leads to an increase in the turbulence intensity near the bed. Additionally, as illustrated in Fig. 9, many irregularities are observed upstream and downstream of the abutment due to the primary vortex's shuddering effect and the shedding of the wake vortices. Dey and Barbhuiya (2006) marked a rapid convexity in turbulence intensity profiles and attributed it to the flow separation and eddy vortices around the abutment.

The presence of vegetation in the channel bed introduces additional complexity due to the interaction between the flow and the vegetation. Upstream of the abutment, the lowest levels of turbulence intensity were noticed, and the turbulence intensity increased as the flow moved downstream of the abutment. Turbulence intensity reached its maximum value near the abutment's downstream corner. Typically, the presence of vegetation in the bed led to an increase in turbulence intensities near the bed. Results showed that, regardless of the arrangement pattern of vegetation elements, the turbulence intensity increases with the vegetation density. In fact, the turbulence introduced in the wake zone of each vegetation element enhances the overall turbulence intensity around the abutment. The highest turbulence intensity has been found for higher vegetation density of $\lambda = 0.161$ arranged in a square configuration.

In the presence of bed vegetation, under ice-covered flow conditions, the turbulence intensity around the abutment does not follow any specific trend. As shown in Fig. 10, flow behavior around the abutment is very complex due to the combined effects of ice cover, bridge abutment, and vegetation patches with different densities and arrangement patterns. The additional irregularities in the flow caused by different ice cover roughness and vegetation arrangement can disrupt the flow patterns, leading to enhanced turbulence intensity. As a result of the interaction of these factors, the patterns of turbulence intensity are non-uniform and practically unpredictable. However, it can be observed that the streamwise turbulence intensity in the zone upstream of the abutment has a decreasing trend with the increase in the distance from the bed. In this context, the turbulent fluctuations near the channel bed take precedence over those near the water surface. Given that the primary sediment transport mechanisms driven by drag forces resulting from vegetation elements and bed shear stress, predominantly occur near the bed (Yager and Schmeckle, 2013), it can be inferred that the ADV's inability to measure fluctuations near the water surface has a minimal

impact on the overall results.

3.2. Reynolds Shear stress

Reynolds Shear Stress (τ_r) is an important parameter for calculating the momentum transfer between the water and the channel boundaries. Understanding the distribution of Reynolds shear stress is essential in different aspects of river flow analysis, including bed erosion and deposition, sediment transport, hydraulic modeling, and flow resistance. Although sediment transport is not within the objective of this study, it is crucial to evaluate the Reynolds shear stress in order to assess the effect of the redistribution of flow and turbulence on channel boundaries. Reynolds shear stress can be calculated using Eqs. (8) and (9).

$$\langle u'w' \rangle = \frac{1}{N} \sum_{i=1}^N (u - \bar{u})(w - \bar{w}) \quad (8)$$

RSS is normalized by the bed shear stress at $z/H = 0$ (τ_{bed}) as following,

$$\frac{\tau_r}{\tau_{bed}} = \frac{-\rho \langle u'w' \rangle}{\rho u_*^2} = \frac{-\langle u'w' \rangle}{u_*^2} \quad (9)$$

The contour maps of the dimensionless Reynolds shear stress (RSS) for open channel flow in the presence and absence of bed vegetation are presented in Fig. 11. As indicated in Fig. 11, RSS reached the maximum values near the downstream corner of the abutment.

Flow separation near the abutment results in a recirculation zone behind the abutment and the development of vortices, which can lead to velocity gradients and turbulent fluctuations that finally contribute to the development of RSS. In the recirculation zone, the flow moves opposite to the main flow, resulting in significant variations in Reynolds shear stress. The maximum values of $\frac{\langle u'w' \rangle}{u_*^2}$ were observed downstream of the abutment where the secondary vortices happen. As pointed out by Melville (1992), secondary vortices can be generated near the primary vortex, behind the abutment, and at the separation zone, limiting the power of the primary vortex in the development of a scour hole. Downstream of the abutment, RSS under an open flow condition decreases in the direction away from the bed, with negative values observed at flow depths above $z/H = 0.3$, as illustrated in Fig. 12. These

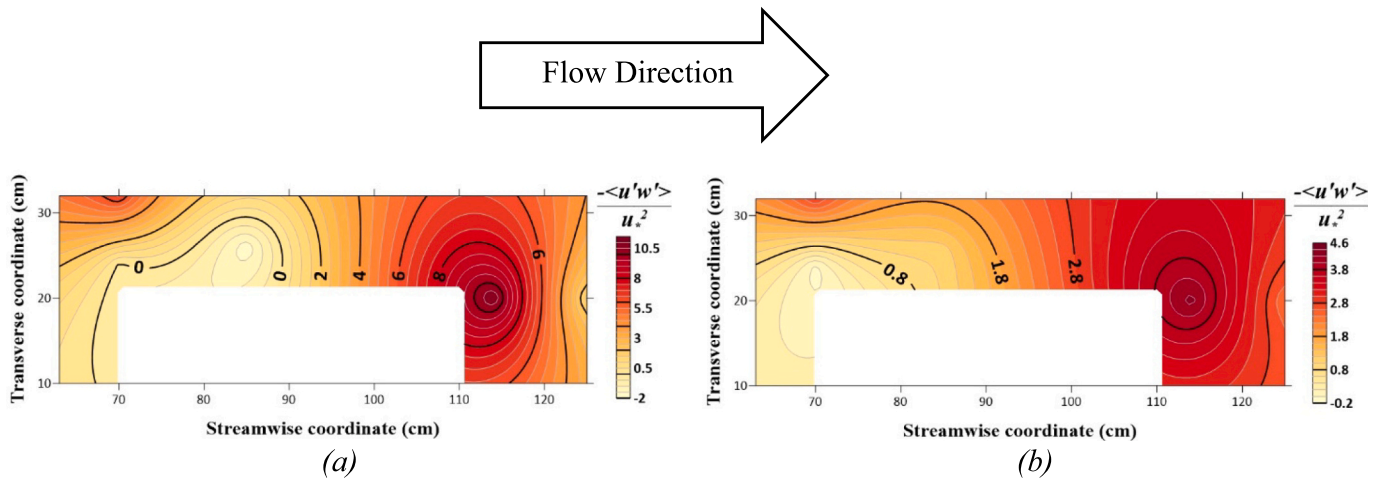


Fig. 11. Contour maps of normalized streamwise Reynolds shear stress around the abutment under open channel flow conditions in vegetated bed at flow depth $z/H = 0$ for: (a) vegetation arranged in a square configuration with lower density, and (b) vegetation arranged in a staggered configuration with lower density.

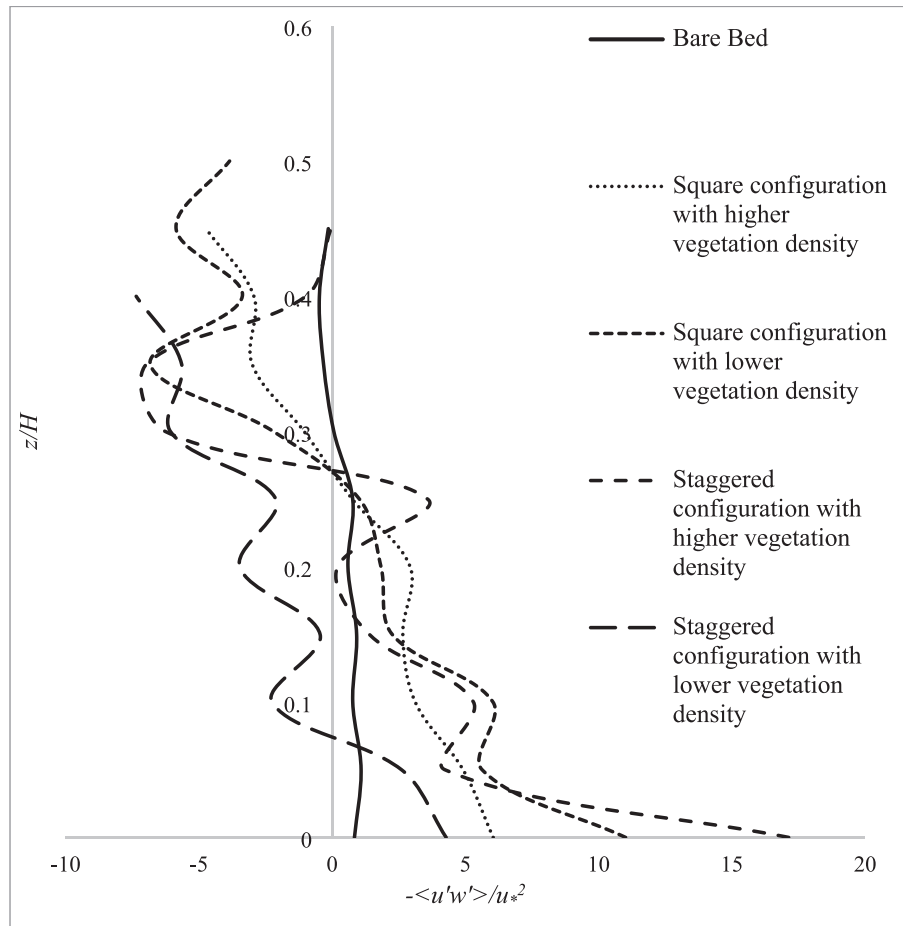


Fig. 12. Vertical distribution of Reynolds shear stresses downstream of the abutment (location 6) for various vegetation arrangements in the bed under open flow conditions.

negative RSS values are due to vegetation morphology that produces turbulent fluxes and negative velocity gradients. The presence of a bed vegetation patch led to changes in RSS vertical distribution from an upright profile with minor changes to a declining nonlinear trend. The results of this study are in good agreement with the findings of Afzali-mehr et al. (2011) who observed that the Reynolds stress distribution in channels with submerged vegetated bed was nonlinear due to the drag

force caused by vegetation.

The presence of bed vegetation caused an increase in RSS values near the bed. The RSS decreased to zero at the flow depth of about $z/H = 0.3$, and then, as z/H increased, it reached negative values depending on the vegetation arrangement and density. The main reason for this change is the flow partitioning caused by the bed vegetation that separates the flow into different pathways through the gaps between vegetation

elements, resulting in the change of velocity gradients. Thus, the profiles of shear stress distribution and spatial variations of RSS were modified compared to those of flow in a channel without bed vegetation. It can also be assumed that each vegetation element acts as a flow barrier, and the von Kármán vortex street created behind vegetation elements causes disturbances in flow patterns. From the distribution profiles of turbulence intensity, Reynolds stress, and streamwise velocity, it can be concluded that the zones with the maximum turbulence intensity and Reynolds shear stresses coincide with the regions having the highest velocity gradient.

The positive RSS values in the normalized profiles indicate the erosion zone, and negative values represent the deposition zone (Karami et al., 2018). The results of observations indicate that the higher positive values of RSS occurred close to the bed ($z/H = 0$) in the vicinity of the abutment. This result suggests that a significant portion of the area around the abutment is prone to erosion. The smaller positive values are observed in the staggered configuration with lower vegetation density, as illustrated in Fig. 11, implying a lower anticipated level of bed erosion in this particular scenario.

The RSS distribution around the abutment in vegetated bed under ice-covered flow conditions is depicted in Fig. 13. The distribution patterns of RSS in the presence of ice cover, particularly in the rough cover case, exhibit substantial differences from those observed under the open channel flow conditions, indicating a much more pronounced effect of the ice cover on the RSS values compared to that of the leafless bed vegetation configurations examined herein. Reynolds shear stress depends on the velocity fluctuation components. According to Eq. (9), negative RSS values mean that the product of velocity fluctuations in the longitudinal direction and velocity fluctuations in the transverse

direction has become positive. This means that either both velocity fluctuations are positive or both are negative. In other words, velocity fluctuations in both longitudinal and transverse directions are either higher or lower than the average values of velocity fluctuations in both directions. Thus, under the rough ice-covered condition, an enlarged zone for negative RSS values at $z/H = 0$ downstream of the abutment can be attributed to the simultaneous increase of streamwise and transverse velocity fluctuation values that were observed in profiles of velocity distributions in both directions.

3.3. Turbulent Kinetic Energy (TKE)

Specific turbulent kinetic energy (TKE) is the energy transferred and dissipated within turbulent flows. It is often used to describe and predict various phenomena, such as how flow interacts with structures and elements. In a vegetated channel, the dominant turbulent energy is generated by the vegetation patch rather than the sand bed, and the correlation between shear stress and TKE varies (Rehman and Hong, 2022). The TKE can be determined using Eq. (10).

$$TKE = \frac{1}{2} (u_{RMS}^2 + v_{RMS}^2 + w_{RMS}^2) \quad (10)$$

According to reported results, the presence of vortices indicates a sharp increase in TKE (Liu and Nepf, 2016; Ortiz et al., 2013). In the wake region of the abutment, vortices and flow separation contribute to turbulence and TKE enhancement. The flow reattachment to the abutment wall in the recirculation zone can create complex flow patterns and enhance turbulence levels near the wall, leading to an increase in TKE. Besides, velocity gradients, shear layers, and flow instabilities can be

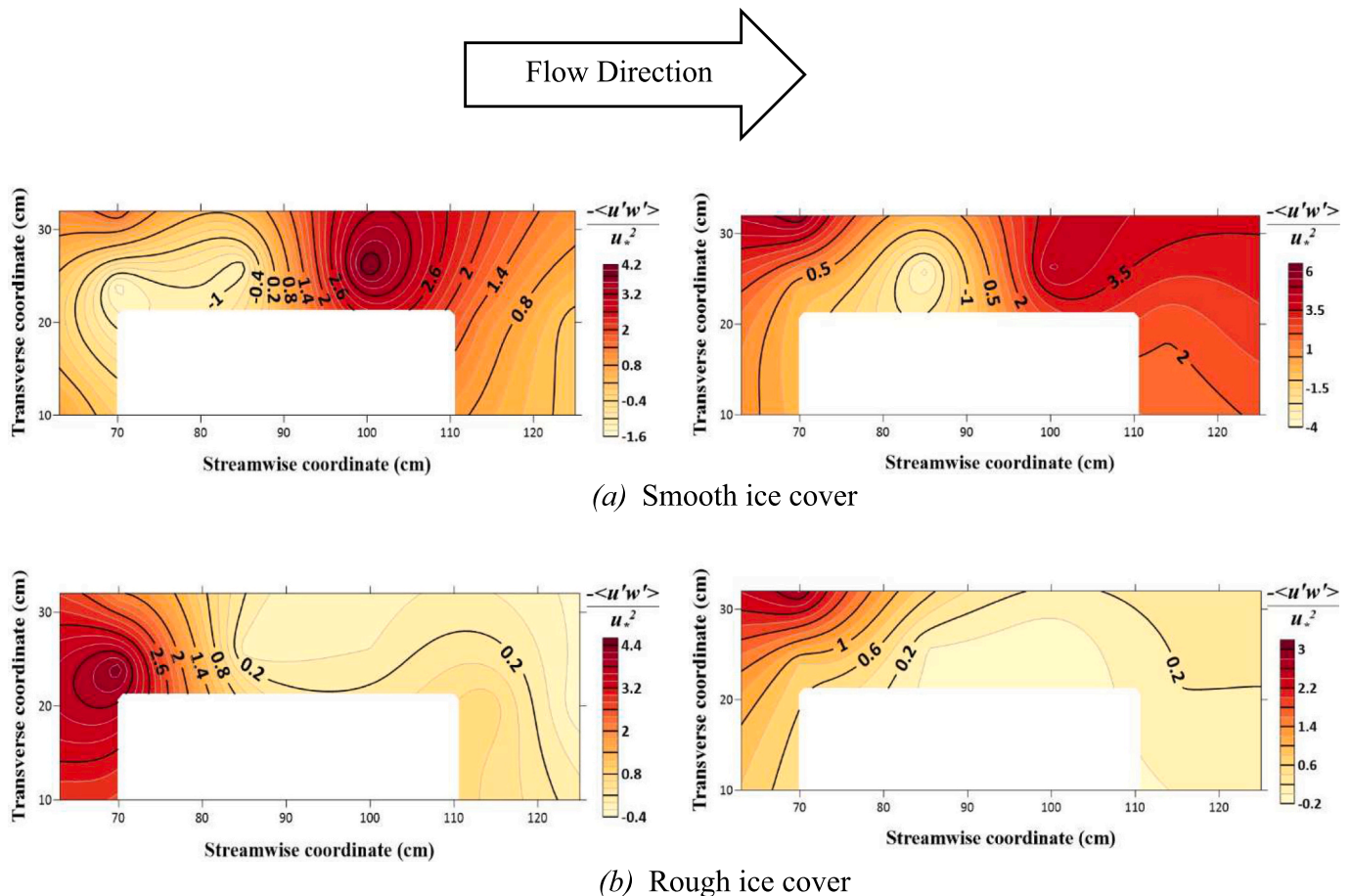


Fig. 13. Contour maps of normalized streamwise Reynolds shear stress around abutment at the depth of $z/H = 0$ under ice-covered flow conditions in vegetated channel with lower vegetation density arranged in a square pattern (left panels) and lower vegetation density arranged in a staggered pattern (right panels).

generated due to the interaction between the approaching flow and the abutment, which, in turn, can increase TKE near the abutment. Results of experiments in the presence of vegetation in the bed showed an enhancement in TKE values around the abutment compared to that of the bare bed. Vortices are created as the flow encounters vegetation elements. These vortices mix the fluid, resulting in enhanced turbulence levels and TKE.

Fig. 14 shows the TKE contours for flows under different vegetation arrangements and open flow conditions, and Fig. 15 compares the vertical distributions of TKE in different vegetation configurations under open and ice-covered flow conditions downstream of the abutment. In all cases illustrated in Fig. 15a, the TKE exhibits an increasing trend with distance from the bed. Even though the turbulent kinetic energy near the bed is larger in the cases with vegetation than that without vegetation in the channel bed, it reaches the same level at a certain distance of about $z/H = 0.4$ from the bed regardless of the bed surface conditions. This means that, in the presence of bed vegetation, the range of changes in energy across the flow depth is less than that of the bare bed.

Furthermore, the observations revealed that the vegetation density and TKE had an opposite relationship; namely, the decrease in vegetation density led to an increase in the TKE value. Dense vegetation with a smaller spacing distance between vegetation elements causes a greater sheltering effect than sparse vegetation, as explained by Raupach (1992), and thus results in a lower TKE value. At least one peak in the TKE profiles is observed depending on the location around the abutment and the layout of the vegetation elements. Variations in layout patterns of vegetated elements and the sharp deflections in velocity profiles explain the differences in the specific flow depths at which the TKE peaks occur (Nosrati et al., 2022). For instance, in the vegetated bed cases, one TKE peak is associated with the velocity change due to moving from the sheath layer to the higher depths of the flow.

Results of comparison in Figs. 12 and 15 show that TKE and Reynolds stress profiles do not follow a similar distribution trend. Thus, in addition to the Reynolds stress, the TKE distribution should be assessed when the flow structure around the abutment in the presence of vegetation is investigated. The presence of vegetation under ice-covered conditions causes different patterns of velocity profiles, and, thus, different TKE distributions, comparing to those of open channel flow. Fig. 15b illustrates the TKE profiles in the presence of vegetation downstream of the abutment under smooth and rough ice-covered conditions. Under ice-covered flow conditions, TKE profiles initiate almost from zero in close proximity to the bed. The effect of ice cover on the TKE near the bed is opposite to the effect of vegetation stems. Subsequently, the TKE profiles for various vegetation arrangements exhibit a diverging

increasing trend until reaching their maximum values, followed by a converging decreasing trend toward the ice cover. Notably, at a specific depth of approximately $z/H = 0.4$, the TKE profiles gain nearly a constant value across all cases downstream of the abutment. It is noteworthy that this consistent TKE value at $z/H = 0.4$ under ice-covered conditions is approximately half of the corresponding value in open channel flow. This underscores a notable reduction in TKE magnitudes under ice-covered conditions. Typically, the TKE value is reduced near the ice cover-water interface due to the dampening effect of the ice cover. This reduction in TKE is caused by a reduced mixing process between water layers. The increased resistance resulting from the rough cover dampens the turbulence and reduces the TKE near ice cover. The rough ice cover can also prevent the development of large-scale turbulent structures. The upper section of the TKE profiles in the open flow condition reveals an increasing trend, distinctly contrasting that of the ice-covered flow conditions where the graphs exhibit a descending trend toward the ice cover.

The total turbulent kinetic energy (TKE) is comprised of contributions from three directions, namely, streamwise, transverse, and vertical directions. The contribution from each direction plays a vital role in shaping the river dynamics. Assessment of the contributions of TKE in different directions provides valuable insights into turbulence patterns and energy dynamics within the channel. The ratio of TKE contributions in the streamwise direction to total TKE (R_x) can be estimated using Eq. (11).

$$R_x = \frac{u_{RMS}^2}{u_{RMS}^2 + v_{RMS}^2 + w_{RMS}^2} \quad (11)$$

The ratio of TKE contributions in the transverse direction to total TKE (R_y , Eq. (12)), representing the energy associated with the lateral flow across the channel's width, is also essential to characterize the energy dissipation and momentum exchange in this direction.

$$R_y = \frac{v_{RMS}^2}{u_{RMS}^2 + v_{RMS}^2 + w_{RMS}^2} \quad (12)$$

In addition, TKE contributions in the vertical direction that represents the flow energy associated with the vertical motion, such as upward and downward movement of water, is an important factor in turbulent flows around in-stream infrastructures, and areas with rapid velocity changes across the depth. The ratio of TKE contributions in the vertical direction (R_z) can be computed using Eq. (13).

$$R_z = \frac{w_{RMS}^2}{u_{RMS}^2 + v_{RMS}^2 + w_{RMS}^2} \quad (13)$$

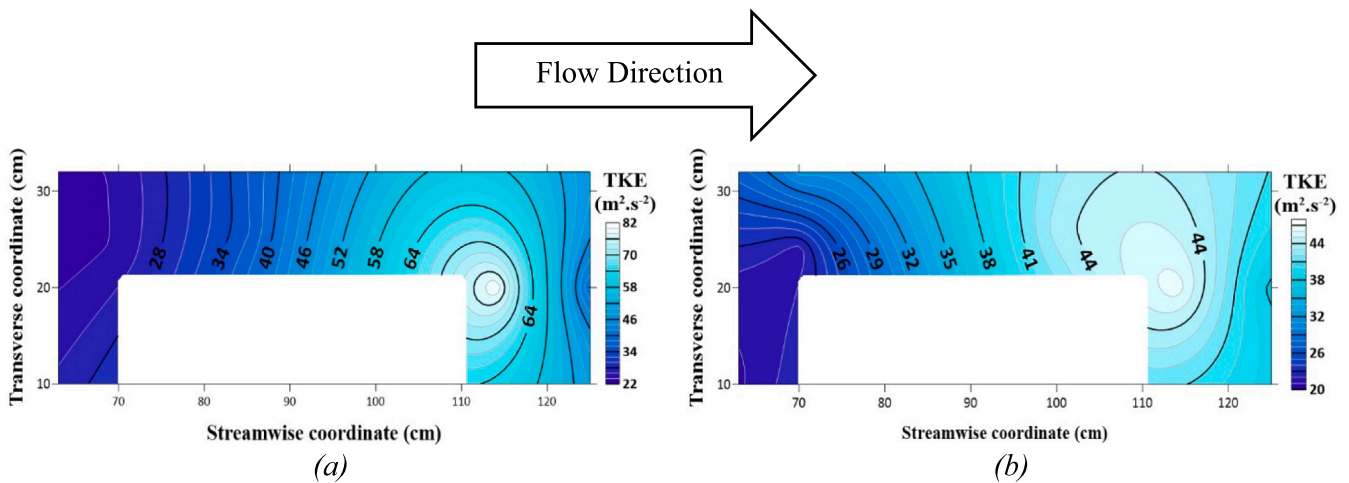


Fig. 14. Contour maps of turbulent kinetic energy (TKE) around the abutment under open channel flow conditions for vegetated bed at the flow depth of $z/H = 0$ with (a) lower density of vegetation arranged in a square configuration, and (b) vegetated bed with lower density of vegetation arranged in a staggered configuration.

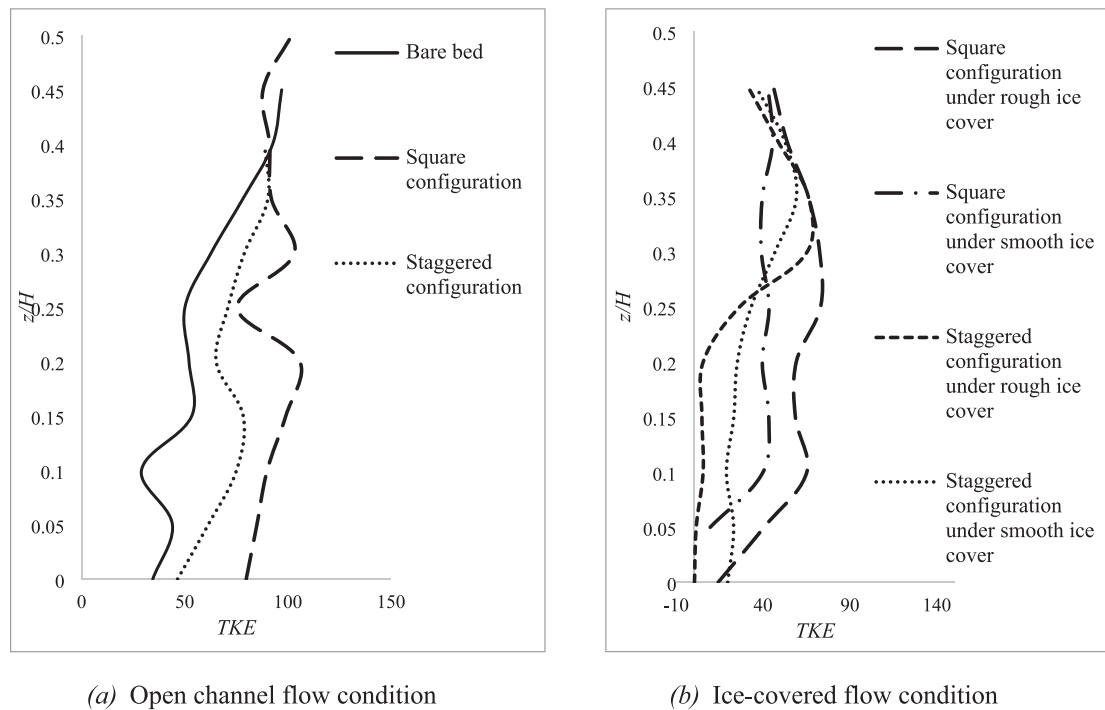


Fig. 15. The vertical distribution of TKE for the bare bed and vegetated bed with different vegetation configurations and lower vegetation density downstream of the abutment (location 6) for (a) open channel flow conditions and (b) ice-covered flow conditions.

Fig. 16 illustrates the distribution of R_x , R_y , and R_z around the abutment at $z/H = 0$, considering the influence of vegetation under the rough ice-covered flow condition. The ratio of streamwise TKE contributions to the total TKE plays a critical role, constituting 40% to 80% of the total TKE at various locations around the abutment. This highlights the significance of R_x in driving the flow downstream. On the other hand, depending on the specific location and the vegetation arrangements, R_y typically accounts for approximately 15% to 50% of the total TKE. The remaining portion of the total TKE that is attributed to the TKE in the vertical direction (R_z) has the lowest magnitudes, accounting for up to 30% of the total TKE. While it is less dominant compared to the streamwise and lateral directions, R_z still plays an important role in sediment transport within the water column and the vertical mixing of water.

Fig. 16 shows an inverse relationship between R_x and R_y values. When the TKE contribution in the streamwise direction reaches its peak, the TKE contribution in the transverse direction simultaneously reaches its lowest value. This phenomenon demonstrates the complementary nature of TKE between these two directions, with a high TKE in one direction coinciding with a low TKE in the perpendicular direction. Additionally, a pattern between the peak values of R_x and the lowest values of R_z is observed. Remarkably, the peak R_x values occur at the exact location where the lowest values of R_z are observed. This alignment suggests a potential correlation between the vertical motion near the abutment and the flow dynamics in the streamwise direction.

4. Conclusion

This study aimed to investigate the characteristics of turbulent flow around a rectangular abutment in the presence of vegetation in the channel bed while considering the simultaneous impacts of ice cover floating on the water surface. The complex interactions between flow, vegetation, and ice cover have been studied based on laboratory experiments considering different ice cover roughness, vegetation layout patterns, and vegetation densities. Results showed that the vegetation configuration has a greater effect on velocity distribution compared to

vegetation density. It appears that the square configuration of vegetation elements in the bed enhances flow velocity by channeling and directing the flow between the rows of vegetation elements, whereas the staggered configuration of vegetation elements in the bed interferes with the flow, leading the velocity to decrease. In open channel flow, the velocity profile shows an S-shaped curve, while under ice-covered flow conditions, the velocity profiles take on a convex shape. In addition to the first peak of velocity profiles occurring in the sheath layer of vegetation, under ice-covered flow conditions, the second peak of velocity profiles is located between vegetation canopy and ice cover. The location of the second peak is affected by the roughness of vegetation canopy and ice cover.

The turbulence intensity levels are lower upstream of the abutment and higher downstream, peaking near the downstream corner. The turbulence is generally amplified by the bed vegetation, and higher vegetation density results in increased turbulence regardless of the arrangement pattern of vegetation elements. Different roughness of the ice cover and vegetation disrupt flow patterns, causing non-uniform and unpredictable turbulence.

In open channel flow, the maximum Reynolds shear stress (RSS) values were observed in the region downstream of the abutment where secondary vortices occur. The presence of bed vegetation influenced the vertical distribution of RSS, with increased RSS values near the bed and a decline to zero around $z/H = 0.3$, followed by negative values. A higher vegetation density leads to an increased RSS value. Under an ice-covered flow condition, particularly under rough ice-covered flow conditions, the effect of ice cover on RSS values was more evident than that of the leafless vegetation in the channel bed. Under the rough ice-covered condition, an enlarged zone for the negative RSS values downstream of the abutment can be attributed to the increased velocity fluctuations in both streamwise and transverse directions. Under an ice-covered flow condition, the RSS distributions showed dramatic changes compared to those in an open channel flow. The zones with the maximum turbulence intensity and Reynolds shear stresses coincide with the regions having the highest velocity gradient.

The bed vegetation significantly enhances the TKE around the

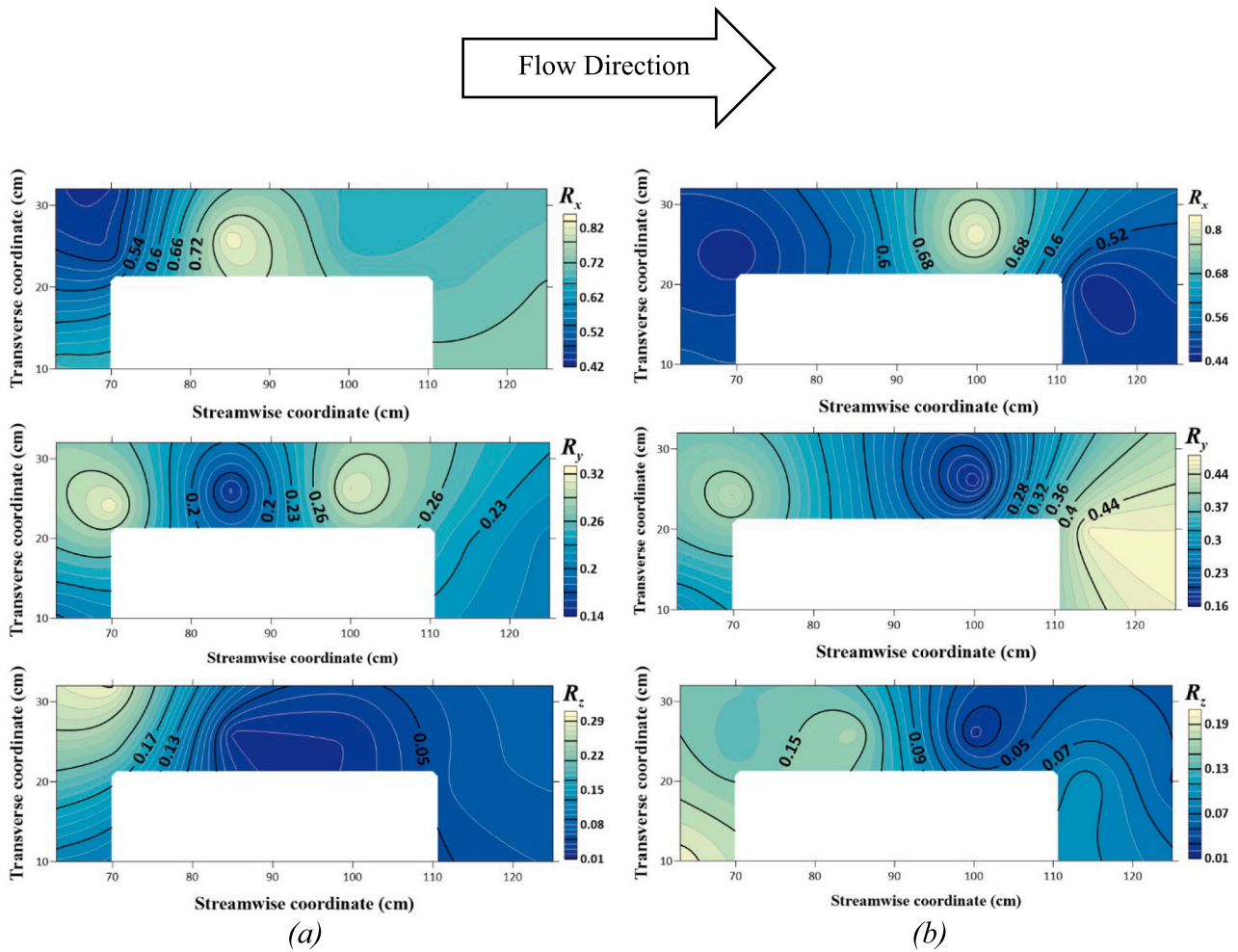


Fig. 16. Contour maps of the ratio of TKE contributions in the streamwise (R_x), transverse (R_y), and vertical (R_z) directions around the abutment under the rough ice-covered flow condition at the flow depth of $z/H = 0$ for (a) vegetated bed with lower density of vegetation arranged in a square configuration, and (b) vegetated bed with lower density of vegetation arranged in a staggered configuration.

abutment, with the TKE values inversely related to the vegetation density. In open flow conditions, in particular, for the square configuration of vegetation in the bed, the TKE profile shows higher values near the bed than of ice-covered conditions. Notably, the TKE under ice-covered conditions has substantially lower magnitudes than that in open flow conditions. This study uncovers the critical role of streamwise TKE (R_x), constituting up to 80% of total TKE. An inverse relationship between R_x and R_y values highlights their complementary nature. When the TKE contribution in the streamwise direction reaches its peak, the TKE contribution in the transverse direction simultaneously reaches its lowest value.

The overall impact of vegetation and ice cover on turbulent flow characteristics cannot be predetermined, as each case should be evaluated individually using appropriate methodologies. The effect of vegetation depends on specific vegetation attributes, including mechanical characteristics. The impacts of ice cover on the characteristics of turbulent flow also depend on the type of ice cover (such as sheet cover or ice jam) since different types of ice cover have different roughness. Experimental studies inevitably face limitations, and this research is not an exception. One noteworthy limitation pertains to the ADV utilized, which had constraints in recording data at shallower depths. Consequently, velocity measurements were confined to the deeper sections of the flow. While the inability to directly assess the near-surface (near water surface or ice cover) velocity data may limit the spatial coverage and the comprehensive understanding of flow dynamics, quantitative modeling, and simulation approaches can be employed to estimate these

parameters using the data provided by this study. These predictive methods can help fill the gaps in data and provide insights into complex flow patterns and interactions with the channel bed, bed vegetation, and ice cover, offering a more holistic view of the study area.

Funding

The Natural Sciences and Engineering Research Council of Canada (NSERC) under the Discovery Grant Program RGPIN-2019-04278.

Author statements

The authors declare no conflict of interest.
The authors declare that they have NOT used any AI tools for preparing this paper.

Dr. Jueyi Sui, P.Eng.
Corresponding Author, on behalf of all co-authors.
Professor.
School of Engineering.
University of Northern British Columbia.
3333 University Way, Prince George.
British Columbia, Canada, V2N 4Z9.
Tel. (250) 960-6399; Fax: (250) 9605845.
Email: jueyi.sui@unbc.ca
Website: www2.unbc.ca/jueyi-sui

CRedit authorship contribution statement

Sanaz Sediqi: Writing – original draft, Validation, Software, Methodology, Investigation, Formal analysis, Data curation, Conceptualization. **Jeuyi Sui:** Writing – review & editing, Writing – original draft, Validation, Supervision, Resources, Project administration, Methodology, Investigation, Funding acquisition, Formal analysis, Conceptualization. **Guowei Li:** Validation, Methodology, Investigation, Data curation. **Mauricio Dziedzic:** Writing – review & editing, Validation, Supervision, Conceptualization.

Declaration of competing interest

The authors declare no conflict of interest.

Data availability

Data will be made available on request.

References

- Afzalimehr, H., Rennie, C.D., 2009. Determination of bed shear stress in gravel-bed rivers using boundary-layer parameters. *Hydrol. Sci. J.* 54 (1), 147–159. <https://doi.org/10.1623/hysj.54.1.147>.
- Afzalimehr, H., Moghbel, R., Gallichand, J., Sui, J., 2011. Investigation of turbulence characteristics in channel with dense vegetation. *International Journal of Sediment Research* 26 (3), 269–282. [https://doi.org/10.1016/S1001-6279\(11\)60093-0](https://doi.org/10.1016/S1001-6279(11)60093-0).
- Afzalimehr, H., Bakhshi, S., Gallichand, J., Sui, J., 2014. Effect of vegetated-banks on local scour around a wing-wall abutment with circular edges. *J. Hydrodyn.* 26 (3), 447–457. [https://doi.org/10.1016/S1001-6058\(14\)60051-2](https://doi.org/10.1016/S1001-6058(14)60051-2).
- Ahmed, F., Rajaratnam, N., 2000. Observations on Flow around Bridge Abutment. *J. Eng. Mech.* 126 (1), 51–59. [https://doi.org/10.1061/\(ASCE\)0733-9399\(2000\)126:1\(51\)](https://doi.org/10.1061/(ASCE)0733-9399(2000)126:1(51)).
- Barahimi, M., Sui, J., 2023. Effects of Submerged Vegetation Arrangement patterns and Density on Flow Structure. *Water* 15 (1), 176. <https://doi.org/10.3390/w15010176>.
- Barbhuiya, A.K., Dey, S., 2003. Vortex Flow Field in a Scour Hole around Abutments. *International Journal of Sediment Research* 18 (4).
- Boylan, C.W., Sheldon, R.B., 1976. Submerged Macrophytes: growth under Winter Ice Cover. *Science* 194 (4267), 841–842. <https://doi.org/10.1126/science.194.4267.841>.
- Caroppi, G., Västilä, K., Gualtieri, P., Järvelä, J., Giugni, M., Rowiński, P.M., 2020. Acoustic Doppler velocimetry (ADV) data on flow-vegetation interaction with natural-like and rigid model plants in hydraulic flumes. *Data Brief* 32, 106080. <https://doi.org/10.1016/j.dib.2020.106080>.
- Chen, S.-C., Kuo, Y.-M., Li, Y.-H., 2011. Flow characteristics within different configurations of submerged flexible vegetation. *J. Hydrol.* 398 (1–2), 124–134. <https://doi.org/10.1016/j.jhydrol.2010.12.018>.
- Dey, S., Barbhuiya, A.K., 2006. Velocity and turbulence in a scour hole at a vertical-wall abutment. *Flow Meas. Instrum.* 17 (1), 13–21. <https://doi.org/10.1016/j.flowmeasinst.2005.08.005>.
- D'Ippolito, A., Calomino, F., Penna, N., Dey, S., Gaudio, R., 2022. Simulation of Accelerated Subcritical Flow Profiles in an Open Channel with Emergent rigid Vegetation. *Appl. Sci.* 12 (14), 6960. <https://doi.org/10.3390/app12146960>.
- Dittrich, A., Järvelä, J., 2005, July 1. Flow vegetation sediment interaction. *Water Engineering Research | Korea Science* 6 (3), 123–130. <https://koreascience.kr/article/JAKO200518718187276.page>.
- Ettema, R., 2002. Review of Alluvial-channel responses to River Ice. *J. Cold Reg. Eng.* 16 (4), 191–217. [https://doi.org/10.1061/\(ASCE\)0887-381X\(2002\)16:4\(191\)](https://doi.org/10.1061/(ASCE)0887-381X(2002)16:4(191)).
- Ettema, R., Fujita, I., Muste, M., Kruger, A., 1997. Particle-image velocimetry for whole-field measurement of ice velocities. *Cold Reg. Sci. Technol.* 26 (2), 97–112. [https://doi.org/10.1016/S0165-232X\(97\)00011-6](https://doi.org/10.1016/S0165-232X(97)00011-6).
- Giacomazzo, M., Bertolo, A., Brodeur, P., Magnan, P., 2023. Relationship between submerged aquatic vegetation, turbidity, and fish distribution in a large shallow fluvial lake. *Environ. Biol. Fish* 106 (1), 1–17. <https://doi.org/10.1007/s10641-022-01359-w>.
- Hanis, D., Zabilansky, L., 2004. Laboratory Test of Scour under Ice: Data and Preliminary Results [R]. US Army CREEL Research Report, Tr-04-09, pp. 77–118.
- Heller, V., 2011. Scale effects in physical hydraulic engineering models. *J. Hydraul. Res.* 49 (3), 293–306. <https://doi.org/10.1080/00221686.2011.578914>.
- Huai, W., Zhang, J., Katul, G.G., Cheng, Y., Tang, X., Wang, W., 2019. The structure of turbulent flow through submerged flexible vegetation. *J. Hydrodyn.* 31 (2), 274–292. <https://doi.org/10.1007/s42241-019-0023-3>.
- Jafari, R., Sui, J., 2021. Velocity Field and Turbulence Structure around Spur Dikes with Different Angles of Orientation under Ice Covered Flow Conditions. *Water* 13 (13), 1844. <https://doi.org/10.3390/w13131844>.
- Jing, S., Yang, W., Chen, Y., 2019. Smooth Open Channel with increasing Aspect Ratio: Influence on secondary Flow. *Water* 11 (9), 1872. <https://doi.org/10.3390/w11091872>.
- Kabiri, F., Afzalimehr, H., Sui, J., 2017. Flow structure over a wavy bed with vegetation cover. *International Journal of Sediment Research* 32 (2), 186–194. <https://doi.org/10.1016/j.ijsrc.2016.07.004>.
- Karami, H., Hosseinzadeh, H., Hosseini, K., Ardeshtir, A., 2018. Scour and three-dimensional flow field measurement around short vertical-wall abutment protected by collar. *KSCSE J. Civ. Eng.* 22 (1), 141–152. <https://doi.org/10.1007/s12205-017-0521-1>.
- Kazem, M., Afzalimehr, H., Sui, J., 2021. Characteristics of Turbulence in the Downstream Region of a Vegetation Patch. *Water* 13 (23), 3468. <https://doi.org/10.3390/w13233468>.
- Kothiyari, U.C., Hager, W.H., Oliveto, G., 2007. Generalized Approach for Clear-Water Scour at Bridge Foundation elements. *J. Hydraul. Eng.* 133 (11), 1229–1240. [https://doi.org/10.1061/\(ASCE\)0733-9429\(2007\)133:11\(1229\)](https://doi.org/10.1061/(ASCE)0733-9429(2007)133:11(1229)).
- Li, G., Sui, J., Sediqi, S., Dziedzic, M., 2023. Local scour around submerged angled spur dikes under ice cover. *International Journal of Sediment Research* 38 (6), 781–793. <https://doi.org/10.1016/j.ijsrc.2023.08.003>.
- Lind, L., Nilsson, C., Polvi, L.E., Weber, C., 2014. The role of ice dynamics in shaping vegetation in flowing waters: Ice dynamics and vegetation in flowing waters. *Biol. Rev.* 89 (4), 791–804. <https://doi.org/10.1111/brv.12077>.
- Lindenschmidt, K.-E., Carstensen, D., Fröhlich, W., Hentschel, B., Iwicki, S., Kögel, M., Kubicki, M., Kundzewicz, Z.W., Lauschke, C., Lazarów, A., Łoś, H., Marszelewski, W., Niedzielski, T., Nowak, M., Pawłowski, B., Roers, M., Schläffer, S., Weintrit, B., 2019. Development of an Ice Jam Flood forecasting System for the lower Oder River—Requirements for Real-Time predictions of Water, Ice and Sediment Transport. *Water* 11 (1), 95. <https://doi.org/10.3390/w11010095>.
- Lindenschmidt, K.-E., Alfredeen, K., Carstensen, D., Choryński, A., Gustafsson, D., Halicki, M., Hentschel, B., Karjalainen, N., Kögel, M., Kolarski, T., Kornaś-Dynia, M., Kubicki, M., Kundzewicz, Z.W., Lauschke, C., Malingier, A., Marszelewski, W., Möldner, F., Näslund-Landénmark, B., Niedzielski, T., Zdralewicz, M., 2022. Assessing and Mitigating Ice-Jam Flood Hazards and risks: a European Perspective. *Water* 15 (1), 76. <https://doi.org/10.3390/w15010076>.
- Liu, C., Nepf, H., 2016. Sediment deposition within and around a finite patch of model vegetation over a range of channel velocity. *Water Resour. Res.* 52 (1), 600–612. <https://doi.org/10.1002/2015WR018249>.
- Liu, C., Yan, C., Sun, S., Lei, J., Nepf, H., Shan, Y., 2022. Velocity, Turbulence, and Sediment Deposition in a Channel Partially Filled with a *Phragmites australis* Canopy. *Water Resour. Res.* 58 (8) <https://doi.org/10.1029/2022WR032381>.
- Melville, B.W., 1992. Local Scour at Bridge Abutments. *J. Hydraul. Eng.* 118 (4).
- Melville, B.W., 1997. Pier and Abutment Scour: Integrated Approach. *J. Hydraul. Eng.* 123 (2), 125–136. [https://doi.org/10.1061/\(ASCE\)0733-9429\(1997\)123:2\(125\)](https://doi.org/10.1061/(ASCE)0733-9429(1997)123:2(125)).
- Melville, B.W., Chiew, Y.-M., 1999. Time Scale for Local Scour at Bridge Piers.
- Mo, S., Zhang, X., Tang, Y., Liu, Z., Kettridge, N., 2017. Effects of snails, submerged plants and their coexistence on eutrophication in aquatic ecosystems. *Knowl. Manag. Aquat. Ecosyst.* 418, 44. <https://doi.org/10.1051/kmae/2017034>.
- Molinas, A., Kheireldin, K., Wu, B., 1998. Shear stress around Vertical Wall Abutments. *J. Hydraul. Eng.* 124 (8), 822–830. [https://doi.org/10.1061/\(ASCE\)0733-9429\(1998\)124:8\(822\)](https://doi.org/10.1061/(ASCE)0733-9429(1998)124:8(822)).
- Nabaei, S.F., Afzalimehr, H., Sui, J., Kumar, B., Nabaei, S.H., 2021. Investigation of the effect of Vegetation on Flow Structures and Turbulence Anisotropy around Semi-Elliptical Abutment. *Water* 13 (21), 3108. <https://doi.org/10.3390/w13213108>.
- Nagao, M., Minami, A., Arakawa, K., Fujikawa, S., Takezawa, D., 2005. Rapid degradation of starch in chloroplasts and concomitant accumulation of soluble sugars associated with ABA-induced freezing tolerance in the moss *Physcomitrella patens*. *J. Plant Physiol.* 162 (2), 169–180. <https://doi.org/10.1016/j.jplph.2004.06.012>.
- Namaee, M.R., Sui, J., 2020. Velocity profiles and turbulence intensities around side-by-side bridge piers under ice-covered flow condition. *J. Hydrol. Hydromech.* 68 (1), 70–82. <https://doi.org/10.2478/johh-2019-0029>.
- Nepf, H.M., 2012. Hydrodynamics of vegetated channels. *J. Hydraul. Res.* 50 (3), 262–279. <https://doi.org/10.1080/00221686.2012.696559>.
- Nepf, H.M., Vivoni, E.R., 2000. Flow structure in depth-limited, vegetated flow. *J. Geophys. Res. Oceans* 105 (C12), 28547–28557. <https://doi.org/10.1029/2000JC900145>.
- Nepf, H., White, B., Lightbody, A., Ghisalberti, M., 2007. Transport in aquatic canopies. In: Gayer, Y.A., Hunt, J.C.R. (Eds.), *Flow and Transport Processes with Complex Obstructions*, vol. 236. Springer, Netherlands, pp. 221–250. https://doi.org/10.1007/978-1-4020-5385-6_6.
- Nezu, I., Sanjou, M., 2008. Turbulence structure and coherent motion in vegetated canopy open-channel flows. *J. Hydro Environ. Res.* 2 (2), 62–90. <https://doi.org/10.1016/j.jher.2008.05.003>.
- Nokhbe Zaeim, M., Saneie, M., 2022. Impact of abutments and vegetation cover in the floodplain on scouring around bridge piers: an experimental modeling. *Model. Earth Syst. Environ.* 8 (4), 4467–4474. <https://doi.org/10.1007/s40808-022-01379-6>.
- Nosrati, K., Afzalimehr, H., Sui, J., 2022. Interaction of Irregular distribution of Submerged rigid Vegetation and Flow within a Straight Pool. *Water* 14 (13), 2036. <https://doi.org/10.3390/w14132036>.
- Oliveto, G., Hager, W.H., 2002. Temporal Evolution of Clear-Water Pier and Abutment Scour. *J. Hydraul. Eng.* 128 (9), 811–820. [https://doi.org/10.1061/\(ASCE\)0733-9429\(2002\)128:9\(811\)](https://doi.org/10.1061/(ASCE)0733-9429(2002)128:9(811)).
- Oliveto, G., Hager, W.H., 2005. Further results to Time-Dependent Local Scour at Bridge elements. *J. Hydraul. Eng.* 131 (2), 97–105. [https://doi.org/10.1061/\(ASCE\)0733-9429\(2005\)131:2\(97\)](https://doi.org/10.1061/(ASCE)0733-9429(2005)131:2(97)).
- Ortiz, A.C., Ashton, A., Nepf, H., 2013. Mean and turbulent velocity fields near rigid and flexible plants and the implications for deposition: Vegetation Impact on Flow and Deposition. *J. Geophys. Res. Earth* 118 (4), 2585–2599. <https://doi.org/10.1002/2013JF002858>.
- Peters, M., Dow, K., Clark, S.P., Malenchak, J., Danielson, D., 2017. Experimental investigation of the flow characteristics beneath partial ice covers. *Cold Reg. Sci. Technol.* 142, 69–78. <https://doi.org/10.1016/j.coldregions.2017.07.007>.

- Rameshkumar, S., Radhakrishnan, K., Aanand, S., Rajaram, R., 2019. Influence of physicochemical water quality on aquatic macrophyte diversity in seasonal wetlands. *Appl Water Sci* 9 (1), 12. <https://doi.org/10.1007/s13201-018-0888-2>.
- Raupach, M.R., 1992. Drag and drag partition on rough surfaces. *Bound.-Layer Meteorol.* 60 (4), 375–395. <https://doi.org/10.1007/BF00155203>.
- Rehman, K., Hong, S.H., 2022. Influence of lateral flow contraction on bed shear stress estimation by using measured turbulent kinetic energy. *Exp. Thermal Fluid Sci.* 139, 110742 <https://doi.org/10.1016/j.expthermflusc.2022.110742>.
- Renman, G., 1989. Distribution of littoral macrophytes in a North Swedish riverside lagoon in relation to bottom freezing. *Aquat. Bot.* 33 (3), 243–256. [https://doi.org/10.1016/0304-3770\(89\)90040-5](https://doi.org/10.1016/0304-3770(89)90040-5).
- Shivpure, V., Devi, T.B., Kumar, B., 2016. Turbulent characteristics of densely flexible submerged vegetated channel. *ISH J. Hydraul. Eng.* 22 (2), 220–226. <https://doi.org/10.1080/09715010.2016.1165634>.
- Sui, J., Wang, D., Karney, B., 2000. Sediment concentration and deformation of riverbed in a frazil jammed river reach. *Can. J. Civ. Eng.* 27 (6), 1120–1129.
- Sui, J., Faruque, M.A., Balachandar, R., 2009. Local Scour Caused by Submerged Square jets under Model Ice Cover. *J. Hydraul. Eng.* 135 (4), 316–319. [https://doi.org/10.1061/\(ASCE\)0733-9429\(2009\)135:4\(316\)](https://doi.org/10.1061/(ASCE)0733-9429(2009)135:4(316)).
- Sui, J., Afzalimehr, H., Samani, A.K., Maherani, M., 2010a. Clear-water scour around semi-elliptical abutments with armored beds. *Int. J. Sed. Res.* 25 (3), 233–245. [https://doi.org/10.1016/S1001-6279\(10\)60041-8](https://doi.org/10.1016/S1001-6279(10)60041-8).
- Sui, J., Wang, J., He, Y., Krol, F., 2010b. Velocity profiles and incipient motion of frazil particles under ice cover. *Int. J. Sediment Res.* 25 (1), 39–51.
- Tanino, Y., Nepf, H.M., 2008. Lateral dispersion in random cylinder arrays at high Reynolds number. *J. Fluid Mech.* 600, 339–371. <https://doi.org/10.1017/S0022112008000505>.
- Thellman, A., Jankowski, K.J., Hayden, B., Yang, X., Dolan, W., Smits, A.P., O'Sullivan, A.M., 2021. The Ecology of River Ice. *Journal of Geophysical Research. Biogeosciences* 126 (9). <https://doi.org/10.1029/2021JG006275>.
- Van Veelen, T.J., Fairchild, T.P., Reeve, D.E., Karunarathna, H., 2020. Experimental study on vegetation flexibility as control parameter for wave damping and velocity structure. *Coast. Eng.* 157, 103648 <https://doi.org/10.1016/j.coastaleng.2020.103648>.
- Vandermause, R., Harvey, M., Zevenbergen, L., Ettema, R., 2021. River-ice effects on bank erosion along the middle segment of the Susitna River, Alaska. *Cold Reg. Sci. Technol.* 185, 103239 <https://doi.org/10.1016/j.coldregions.2021.103239>.
- Velle, G., Skoglund, H., Barlaup, B.T., 2022. Effects of nuisance submerged vegetation on the fauna in Norwegian rivers. *Hydrobiologia* 849 (2), 539–556. <https://doi.org/10.1007/s10750-020-04465-x>.
- Virtanen, R., Muotka, T., Saksa, M., 2001. Species richness-standing crop relationship in stream bryophyte communities: patterns across multiple scales: *Species richness in stream bryophyte communities*. *J. Ecol.* 89 (1), 14–20. <https://doi.org/10.1046/j.1365-2745.2001.00513.x>.
- Wu, P., 2015. Local Scour around Bridge Abutments under Ice Covered Conditions. Doctor of Philosophy, University of Northern British Columbia. <https://doi.org/10.24124/2015/bpgub1042>.
- Wu, P., Hirshfield, F., Sui, J., 2014. Further studies of incipient motion and shear stress on local scour around bridge abutment under ice cover. *Can. J. Civ. Eng.* 41 (10), 892–899. <https://doi.org/10.1139/cjce-2013-0552>.
- Wu, P., Hirshfield, F., Sui, J., 2015. Local scour around bridge abutments under ice covered condition – an experimental study. *International Journal of Sediment Research* 30 (1), 39–47. [https://doi.org/10.1016/S1001-6279\(15\)60004-X](https://doi.org/10.1016/S1001-6279(15)60004-X).
- Wu, P., Balachandar, R., Sui, J., 2016. Local Scour around Bridge Piers under Ice-Covered Conditions. *J. Hydraul. Eng.* 142 (1), 04015038. [https://doi.org/10.1061/\(ASCE\)HY.1943-7900.0001063](https://doi.org/10.1061/(ASCE)HY.1943-7900.0001063).
- Wu, C., Wu, S., Wu, X., Zhang, Y., Feng, K., Zhang, W., Zhao, Y., 2023. Hydrodynamics affected by submerged vegetation with different flexibility under unidirectional flow. *Front. Mar. Sci.* 9, 1041351. <https://doi.org/10.3389/fmars.2022.1041351>.
- Yager, E.M., Schmeckle, M.W., 2013. The influence of vegetation on turbulence and bed load transport. *J. Geophys. Res. Earth* 118 (3), 1585–1601. <https://doi.org/10.1002/jgrf.20085>.
- Zabilansky, L.J., 2002. Ice Cover Effects on Bed Scour: Case Studies. *Cold Reg. Eng.* 795–803 [https://doi.org/10.1061/40621\(254\)68](https://doi.org/10.1061/40621(254)68).